

Joona Pesonen

**OPERATIONAL RESERVE NEEDS OF
FUTURE POWER SYSTEM**
Case Finland

Master's thesis
Faculty of Information Technology and Communication Sciences
Examiner: Pertti Järventausta
Examiner: Sami Repo
October 2024

ABSTRACT

Joona Pesonen: Operational Reserve Needs of
Future Power System - Case Finland
Master's Thesis
Tampere University
Electrical Engineering
October 2024

To ensure secure operation of the electrical power system, it is essential to maintain the balance between production and consumption during all times. While achieving this equilibrium requires contribution from a number of different actors, Transmission System Operators (TSOs) have the final responsibility of the real-time balancing. To fulfill this obligation, the TSOs procure reserves from balancing service providers. The need for this procurement arises from unexpected events such as production forecast errors or power plant failures. These reserves are in turn production, consumption and energy storage units that aim to restore the balance by controlling their power exchange with the connecting grid.

Due to the predicted major increase of renewable generation and total demand in the Nordic countries, also the balancing needs are expected to change significantly in the coming years. Based on these projections, the main objective of this thesis is to study the development of Finnish balancing needs between the years 2026-2033. The timescale of analyzed balancing needs is linked to 15-minute average imbalances. This work also creates a process description for assessing the development of balancing needs and estimates the growth potential of production and consumption ramping. In practice, the balancing needs are estimated through a case study, in which a probabilistic approach based on historical forecast and measurement data is applied. The ramping potential, on the other hand, is analyzed by using the hourly market simulation data created originally for the case study.

When comparing the years 2026 and 2033, the analysis predicts a growth of approximately 320 % for the average upward balancing needs. For the downward direction this change is estimated to be nearly 340 %. In this comparison, the average balancing needs of the year 2026 range from 800 MW to 1300 MW, depending on the assumptions made during the estimation process. These assumptions considered forecast accuracy development, market behavior and wind conditions. Besides predicting substantial growth, the analysis suggests that the future balancing needs are highly dynamic and closely tied to the onshore wind power production level. While studying the hourly ramping of production and consumption, the largest ramps in relation to the installed capacity were associated to offshore wind power and photovoltaic (PV) generation. However, when evaluating the ramping in terms of absolute power, onshore wind power had the largest ramps with maximums close to 28 % of the installed capacity.

Although the transition from the balancing needs to the actual reserve procurement of the TSOs is not straightforward, compensating the predicted increase solely with additional reserves is hardly an economically viable option. For this reason, the role of individual market actors will increase significantly in the future. This self-balancing could be implemented through energy storage systems, active trading or operational decisions such as preserving part of the predicted generation for possible forecast errors. Also, making investment decisions that increase the geographical dispersion of wind and PV assets, are beneficial from the self-balancing point of view as they increase the aggregation of forecast errors. To incentivize this favorable development, additional price components could be considered for the imbalance pricing and connection fees.

Keywords: Balancing, frequency restoration reserves, dynamic reserve sizing, machine learning, kernel density estimation

The originality of this thesis has been checked using the Turnitin Originality Check service.

TIIVISTELMÄ

Joona Pesonen: Säättötarpeiden kehittyminen tulevaisuuden sähköjärjestelmässä – tapaustutkimus Suomesta
Diplomityö
Tampereen yliopisto
Sähkötekniikka
lokakuu 2024

Sähköjärjestelmän toiminnan kannalta on välttämätöntä, että tuotanto ja kulutus vastaavat toisiaan joka hetki. Vaikka järjestelmän tasapainottaminen edellyttää useiden eri toimijoiden yhteistyötä, kantaverkkoyhtiöillä on lopullinen vastuu reaaliaikaisesta tasehallinnasta. Täyttääkseen tämän veloitteen kantaverkkoyhtiöt hankkivat reservejä reservitoimittajilta. Tarve reservihankinnalle syntyy reaaliaikaisista säättötarpeista, joita aiheuttavat esimerkiksi tuotannon ennustevirheet sekä voimalaitosviat. Reservit ovat tuotanto- ja kulutuskohteita tai sähkövarastoja, jotka ohjaavat tehoaan sähköjärjestelmän tarpeiden mukaan.

Uusiutuvan sähköntuotannon sekä kokonaiskulutuksen määrän ennustetaan kasvavan tulevina vuosina Pohjoismaissa merkittävästi. Tämän kehityksen odotetaan heijastuvan myös reaaliaikaiseen tasehallintaan, minkä seurauksena diplomityön päätavoitteena on tutkia säättötarpeiden kehitystä Suomessa vuosien 2026–2033 aikana. Työssä analysoidut säättötarpeet liittyvät 15 minuutin keskiarvoisiin tasevirheisiin. Diplomityö luo myös prosessikuvauksen säättötarpeiden kehityksen tutkimista varten sekä arvioi tuotannon ja kulutuksen tehorempien kasvupotentiaalia. Käytännössä säättötarpeita arvioidaan tapaustutkimuksen kautta, jossa sovelletaan historialliseen ennuste- ja mittausdataan perustuvaa todennäköisyyspohjaista lähestymistapaa. Tehomuutosten kasvupotentiaalia analysoidaan puolestaan käyttämällä tapaustutkimusta varten luotua tuntiresoluution markkinasimulaatio dataa.

Vertailtaessa vuosia 2026 ja 2033 keskenään, työn analyysi ennustaa ylössäättötarpeiden kasvavan keskiarvoisesti noin 320 %. Alassäättötarpeiden osalta kasvun arvioidaan olevan lähes 340 %. Tässä vertailussa vuoden 2026 keskimääräiset säättötarpeet vaihtelevat 800 MW ja 1300 MW välillä, riippuen arviointiprosessin aikana tehdyistä oletuksista. Nämä oletukset huomioivat ennustetarkkuuden kehityksen, markkinakäyttäytymisen sekä tuuliolosuhteet. Sen lisäksi että tulokset ennakoivat merkittävää säättötarpeiden kasvua, ne viittaavat siihen, että tulevaisuuden säättötarpeet ovat erittäin dynaamisia ja tiiviisti sidoksissa maatuulivoiman tuotantotasoon. Analysoitaessa tuotannon ja kulutuksen tehomuutoksia havaittiin, että suurimmat tuntien väliset rampit suhteessa asennettuun kapasiteettiin liittyivät merituuli- ja aurinkovoimaan. Kun taas vertailu suoritettiin absoluuttisten tehomuutosten perusteella, maatuulivoima nousi suuruusjärjestyksessä ensimmäiseksi rampeilla, joiden koko oli noin 28 % asennetusta kapasiteetista.

Vaikka säättötarpeiden siirtyminen kantaverkkoyhtiöiden reservihankinnaksi ei ole suoraviivaista, ennustetun kasvun kompensointi yksin reservihankinnan kasvattamisella on tuskin taloudellisesti kannattava vaihtoehto. Tämän seurauksena yksittäisten markkinatoimijoiden rooli tulee kasvamaan tulevaisuudessa merkittävästi. Käytännössä markkinatoimijat voivat vaikuttaa realisoituihin säättötarpeisiin esimerkiksi energiavarastojen, aktiivisen kaupankäynnin sekä operatiivisten päätösten avulla. Esimerkkinä operatiivisista valinnoista on ennustetun tuotannon osittainen varaaminen mahdollisten ennustevirheiden varalle. Myös investointipäätökset, jotka lisäävät tuuli- ja aurinkovoiman maantieteellistä hajautusta, ovat hyödyllisiä toimijakohtaisen tasehallinnan näkökulmasta, koska ne lisäävät ennustevirheiden aggregoitumista. Tämän suotuisan kehityksen edistämiseksi voitaisiin myös harkita uusien hintakomponenttien soveltamista tasesähkön sekä liityntämaksujen yhteydessä.

Avainsanat: Säättötarpeet, taajuuden palautusreservit, dynaaminen reservimitoitus, koneoppiminen, ydinestimointi

Tämän julkaisun alkuperäisyys on tarkastettu Turnitin Originality Check -ohjelmalla.

PREFACE

First, I would like to express my gratitude to Fingrid Oyj for the opportunity to write my master's thesis on this interesting and highly topical subject. Many thanks also to my advisor M. Sc. Väinö Valli for the feedback and support throughout this journey. Additionally, I wish to show my appreciation to the whole supervisor group at Fingrid Oyj for your professional insights on the way. Special thanks also to the experts at Fingrid's Strategic grid planning unit for running the market simulations and providing the required datasets. Furthermore, many thanks to Prof. Pertti Järventausta at Tampere University for supervising my work and providing guidance during the writing process.

Lastly, endless thanks to my friends and family for your love and support during this chapter of my life.

Helsinki, 1.10.2024

CONTENTS

1. INTRODUCTION	1
2. BACKGROUND	3
2.1 Balancing responsibility and imbalance settlement	4
2.2 Electricity market	5
2.3 Imbalance drivers	5
2.3.1 Forecast errors	6
2.3.2 Deterministic imbalances	8
2.3.3 Short-term variability	8
2.3.4 Contingency events	9
2.4 Balancing the power system in real-time	9
2.4.1 Frequency quality defining parameters	10
2.4.2 Frequency containment process	12
2.4.3 Frequency restoration process	15
3. FUTURE POWER SYSTEM	17
3.1 Changes in production and consumption	17
3.2 Electricity market changes	20
3.3 Balancing of the future power system	21
3.4 A brief overview of methodologies used in recent balancing need and dynamic reserve dimensioning studies	23
3.5 Scenario building for the case study	25
4. METHODOLOGY FOR ESTIMATING THE DEVELOPMENT OF BALANCING NEEDS	28
4.1 Overview of the thesis approach	28
4.2 Phase 1: Data sources and processing	31
4.2.1 Data preprocessing	33
4.2.2 Clustering the forecast error data	35
4.2.3 Defining the number of clusters for k-means++ -algorithm	37
4.2.4 Creation of the conditional PDFs	39
4.3 Phase 2: Market simulations	40
4.4 Phase 3: Calculating the balancing needs	41
4.4.1 Forming a joint PDF for the modeled uncertainty factors	42
4.4.2 Applying reliability level for the joint PDF	43
5. CASE STUDY	45
5.1 Testing the created calculation model	45
5.2 Balancing needs in the examined cases	48
5.3 Ramping of production and consumption in the examined cases	54
6. DISCUSSION	58
7. CONCLUSION	62
SOURCES	64
APPENDIX A: HOURLY BALANCING NEEDS	70
APPENDIX B: BALANCING NEED CALCULATION WITHOUT DAY-AHEAD FORECASTS	72
APPENDIX C: BALANCING NEED CALCULATION WITHOUT DAY-AHEAD FORECASTS, DURATION CURVES OF THE RESULTS	74

ABBREVIATIONS AND SYMBOLS

ACE	Area Control Error
ACE OL	Area Control Error Open Loop
AOF	Activation Optimization Function
aFRR	automatic Frequency Restoration Reserve
BRP	Balance Responsible Party
BSP	Balance Service Provider
CDF	Cumulative Distribution Function
CET	Central European Time
CRPS	Continuous Ranked Probability Score
EAM	Energy Activation Market
ENTSO-E	European Network of Transmission System Operators for Electricity
FCP	Frequency Containment Process
FCR-D	Frequency Containment Reserve - Disturbance
FCR-N	Frequency Containment Reserve - Normal
FFR	Fast Frequency Reserve
FRCE	Frequency Restoration Control Error
FRP	Frequency Restoration Process
GCT	Gate Closure Time
GH _{lc}	Global Horizontal clear sky Irradiation
HVDC	High-Voltage Direct Current
ISP	Imbalance Settlement Period
k-NN	k-Nearest Neighbours
LFC	Load Frequency Controller
LFDD	Low Frequency Demand Disconnection
mFRR	manual Frequency Restoration Reserve
NEMO	Nominated Electricity Market Operator
NTC	Net Transfer Capacity
OTC	Over-the-Counter
PDF	Probability Density Function
PV	Photovoltaic
SOA	System Operation Agreement
SOGL	System Operation Guideline
TSO	Transmission System Operator

C	a set of cluster centers
C_{SF}	scaling factor
c	cluster center
d	dimension
Δf	measured frequency deviation
ΔP	difference between scheduled and measured power exchange
ΔP_{ss}	calculated steady-state response
$\Delta P_{7.5s}$	activated power 7.5 seconds after the start of the frequency ramp
$E_{7.5s}$	activated energy 7.5 seconds after the start of the frequency ramp
$\epsilon_{i,t}$	forecast error
$\epsilon_{i,t}^{pu}$	per unit forecast error
$F_{joint PDF}$	CDF of the joint PDF
$f_{consumption,DA}$	consumption day-ahead forecast error PDF
$f_{consumption,1 h}$	consumption 1-hour ahead forecast error PDF
f_g	generator's frequency
$f_{joint PDF}$	joint PDF of the modeled uncertainty sources
f_m	kernel estimator

$f_{\text{offshore wind,DA}}$	offshore wind power day-ahead forecast error PDF
$f_{\text{offshore wind,1 h}}$	offshore wind power 1-hour ahead forecast error PDF
$f_{\text{PV,DA}}$	PV day-ahead forecast error PDF
$f_{\text{PV,1 h}}$	PV 1-hour ahead forecast error PDF
f_s	synchronous frequency
$f_{\text{wind,DA}}$	onshore wind power day-ahead forecast error PDF
$f_{\text{wind,1 h}}$	onshore wind power 1-hour ahead forecast error PDF
f_X	PDF of the random variable X
f_Y	PDF of the random variable Y
f_Z	PDF of the random variable Z
G_m	a set of clusters
H	inertia constant
h_m	bandwidth of the kernel estimator
i	forecast type
J	moment of inertia of the turbine-generator
K	factor used for the FRCE calculation
$K(\cdot)$	kernel smoothing function
k	number of clusters
m	cluster index
N	number of samples in a cluster
n	variable used in the definition of convolution
ω_R	rated mechanical angular velocity
P	a set of datapoints
P_e	electrical power of the generator
P_m	mechanical power of the turbine-generator
p	datapoint
R_{down}	downward balancing needs
R_{up}	upward balancing needs
\mathbb{R}^d	Euclidean space
ρ_{deficit}	probability for power deficit
ρ_{RL}	reliability level
ρ_{surplus}	probability for power surplus
S_R	generator's rated apparent power
σ_m	standard deviation
$\hat{\sigma}_m$	median absolute estimator
t	quarter-hour index
u	evaluation point for the kernel estimator
x	point at the CDF's or PDF's x-axis
$x_{i,t}$	measured 15-minute average power
$\hat{x}_{i,t}$	forecasted 15-minute average power
z	realized ACE OL value

1. INTRODUCTION

Basic principle for operating electrical power system is to maintain the balance between production and consumption within every timescale [1]. When this equilibrium is distorted the system frequency will deviate from its nominal value. In practice, the frequency begins to increase when there is more production than consumption and vice versa if this relation is reversed. The power imbalances themselves are created by a variety of different drives such as forecast errors, contingency events and stochastic load variation [2]. As the operational frequency range of the generation units is limited, large frequency deviations may lead to disconnections from the grid and consequently increase the risk of total or partial system blackout [1].

Within the Nordic synchronous area, Transmission System Operators (TSOs) are responsible for maintaining the power balance during the delivery period [3]. This area consists of the subsystems of Finland, Sweden, Norway and eastern Denmark, which are synchronously interconnected and thus share the same nominal frequency [4]. The balancing responsibility, on the other hand, is based on the European regulation outlined in the System Operation Guideline (SOGL) [3]. On a practical level, the TSOs procure reserves from Balance Service Providers (BSPs) to counteract the real-time imbalances [5]. These reserves are production, consumption and energy storage units that control their power exchange with the grid according to the system needs [1].

In a modern society where almost every function needs electricity, securing reliable power delivery is crucial [6]. On the other hand, the expected growth in electrical consumption driven by both national and European climate policies, leads to increased need of fossil-free generation [7][8]. When combining the predicted growth of consumption and production with the uncertainty related to the intermittent renewable generation, the need for flexibility in the power system will escalate within the coming years [7]. Part of this predicted increase will be also reflected to the TSOs' reserve procurement. For this reason, the main objective of this thesis is to study the development of Finnish balancing needs within the years 2026-2033. Of the different flexibility timescales, this work concentrates on the balancing needs related to the 15-minute average imbalances.

From the TSO's point of view, studying the development of balancing needs is highly beneficial as the obtained results can be used to evaluate the adequacy of designed

control processes and identify upcoming challenges in the system operation. These results will also indicate the potential of dynamic reserve dimensioning in Finland, as the following analysis is performed on an hourly resolution. Besides the main objective, this work outlines a process description for the balancing need assessment, which can be applied later when there is more presentative data available, or the required production and consumption outlooks are updated. Also, the ramping potential of production and consumption is analyzed briefly in this work. Derived from the main and secondary objectives, the research questions of this thesis are following:

1. What kind of balancing needs the scenarios described by the market simulations cause on an annual and hourly basis?
2. What are the main creation mechanisms for the system imbalances and which factors affect their characteristics?
3. How will the ramping of wind generation, photovoltaic production and consumption develop within the scope of this thesis?

As the development of balancing needs has both financial and operational impacts, many entities have studied the topic during recent years [9][10][11]. Compared to the earlier research, the first novelty value of this work arises from the fact that there are no recent studies that have analyzed the development of Finnish balancing needs with an hourly resolution. The second novelty relates to the thesis methodology, which considers the variation in the market participants' activity by using two separate forecasts for modeling wind and photovoltaic (PV) generation and consumption.

In Chapter 2, the current balancing process and different imbalance drivers are reviewed in detail. This section creates a theoretical foundation for the thesis and provides answers to the second research question. Chapter 3 overviews the upcoming changes in the power system, electricity markets and balancing process. Based on these projections, the scenarios analyzed in the latter case study are derived. Chapter 4 describes the created balancing need assessment process, which is built upon a probabilistic approach using conditional forecast error distributions. Chapter 5 presents the obtained results, considering both the development of balancing needs and the ramping of production and consumption. Finally, the last two chapters of this work discuss the meaning and validity of the results and highlight some key findings.

2. BACKGROUND

The link between power imbalances and frequency deviations can be explained through swing equation, which describes the dynamic behavior of a single synchronous generator [12]. When assuming that both the mechanical and electrical angular velocities of the generator are close to their synchronous values, this equation can be written as [12][13]:

$$\frac{df_g(t)}{dt} = \frac{f_s}{2HS_R} [P_m(t) - P_e(t)]. \quad (1)$$

In the previous formula f_g is the generator's frequency, f_s is the synchronous frequency of the connecting grid, S_R is the generator's rated apparent power, P_m is the mechanical power of the turbine-generator and P_e is the electrical power of the generator. The machine's inertia constant H is in turn defined with Equation 2 below:

$$H = \frac{\omega_R J}{2} \cdot \frac{1}{S_R}, \quad (2)$$

where ω_R is the rated mechanical angular velocity of the rotor and J is the moment of inertia of the turbine-generator [12]. From the first equation we can observe that if the mechanical power differs from the electrical power, the generator's frequency will deviate, and the rate of this change depends on the generator's inertia constant and the magnitude of power imbalance [13].

How the introduced equation reflects the system level behavior can be understood by viewing the right-side subtraction as difference between total production and consumption, and replacing the apparent power and inertia constant with equivalent factors representing the sum of all synchronously connected generators and motors [13]. With these modifications, the change of frequency on the left-side of the equation can be seen to present the system level frequency deviations. This adapted equation will also highlight the role of inertia, which is defined as the system's ability to oppose frequency changes through the kinetic energy stored in the rotating masses.

The practical measures taken to fulfil the equilibrium discussed in the previous paragraph and the different responsibilities of this process are discussed with more detail in the following sections. However, as a general overview of the topic, gaining the balance can be seen as a three-step process which consists of pre-delivery actions made by the market participants, real-time balancing conducted by the TSOs and financial settlement of the realized imbalances after the delivery period [5][14].

2.1 Balancing responsibility and imbalance settlement

According to the Finnish electricity market law, market participants are responsible for ensuring that their electricity production and procurement contracts are corresponding to their consumption and delivery contracts during each Imbalance Settlement Period (ISP) [15]. Market actors try to achieve this through production planning and trading, based on forecasts of consumption and variable production. However, due to uncertainties like short-term variation of wind power production and prediction errors of consumption, there will be power imbalances that are not covered by the pre-delivery actions.

To compensate this mismatch, every market participant is required to have an open supplier, whose responsibility is to compensate possible power imbalances of the market party [16]. These open suppliers form a hierarchical chain of open deliveries, where the TSO's Balance Service Unit is the highest party of the chain, and every party under the TSO has one open supplier [17]. Since it is the TSO's responsibility to maintain the power balance during the delivery period, the unbreakable chain of open deliveries ending to the system operator ensures that imbalances of the market parties are compensated [18].

The market participants whose open supplier is the TSO, are called Balance Responsible Parties (BRPs) [14][18]. The BRPs are expected to plan and control their electricity procurements and deliveries, so that their imbalances remain reasonable in contrast to their operational scope [18]. In practice this is done by trading in day-ahead and intraday markets and utilizing bilateral trade between other BRPs inside the bidding zone [5]. Besides pre-delivery balancing, the BRPs are obligated to deliver production plans to the corresponding TSO after the clearing of day-ahead market and update them before the delivery if needed [5][18]. These plans will help the TSOs to design the real-time balancing of the power system [5].

After the delivery period, BRPs have the financial responsibility of the realized imbalances [14]. This liability is based on imbalance settlement, which implementation is carried out by the common operational unit eSett with the authorization of the Nordic TSOs. Within this process, imbalances are calculated for every BRP considering their consumption, production, trades and possible imbalance corrections. After the calculation process, the BRPs are charged according to their computed imbalance volumes. In Finland, the imbalance pricing is based on the price of activated manual Frequency Restoration Reserve (mFRR) and automatic Frequency Restoration Reserve (aFRR), which are discussed with more detail later in this work [19]. Currently the imbalance pricing is done in an hourly resolution, even though the length of the ISP is 15 minutes.

2.2 Electricity market

In the Nordic power system, wholesale electricity trade is facilitated through energy exchange and Over-the-Counter (OTC) market [20]. The energy exchange is managed by Nominated Electricity Market Operators (NEMOs) and it consists of day-ahead and intraday markets [21][22]. The OTC-market refers to all wholesale trade outside the energy exchange and it covers for example the bilateral trade between the market actors [20]. Besides the trading of physical power, there is also a financial market which role is to enable risk management of the market parties against unfavorable price developments.

The day-ahead market is a closed auction in which electricity is traded for every hour of the next day [20]. Based on the estimated needs, the attending parties place their hourly offers by 12:00 Central European Time (CET) for the following day and the bidding zone in question [20][22]. There are total of 11 bidding zones within the Nordic synchronous area of which Finland as whole constitutes one [1]. After the Gate Closure Time (GCT) of the day-ahead market, the NEMOs calculate electricity price for each bidding zone subject to the made offers and available transmission capacity [22]. If no congestions occur, the electricity price is same for the whole Nordic area and matches the definition of so-called system price [20]. However, when the transmission capacity is insufficient between the areas, the price will be higher than the system price in the deficit bidding zones and lower in the surplus areas.

The role of intraday market is to enable corrective actions in the case of new sale or procurement needs, which arise from events such as changed weather conditions or power plant failures [22]. The intraday market opens after the clearing of day-ahead market and involves both continuous trading and three separate auction rounds [22][23]. In Finland, the GCT for the continuous market is currently 30 minutes before the delivery for the Estonian border, 60 minutes for the Swedish border and equal to the beginning of the delivery period for the domestic trade [22]. The last intraday auction is in turn cleared around 10:00 CET within the day of delivery [23]. The Market Time Unit (MTU) for the domestic trade in Finland is 15-minutes for both intraday auction and continuous market, but the cross border-trade is done with hourly resolution [22][24].

2.3 Imbalance drivers

Since this work is concentrated on determining the balancing needs of future power system, understanding the drivers behind system level imbalances is crucial. For this reason, this chapter introduces the most significant imbalance sources in the Nordic synchronous area and describes their internal characteristics. While reading this chapter, it

is good to note that the absolute sum of different imbalance sources is usually larger than the actual balancing needs due to imbalance netting inside the synchronous area [25]. The extent in which this netting is possible, is dependent on the Available Transmission Capacity (ATC) between different areas of the power system.

The main imbalance drivers can be roughly divided into three categories: forecast errors, deterministic drivers and contingency events [2][26]. Besides to these drivers, stochastic variation of consumption and production is creating imbalances within timescales of few minutes or shorter. Before characterizing the properties of different imbalance drivers in more detail, an overview is given in Figure 1 below.

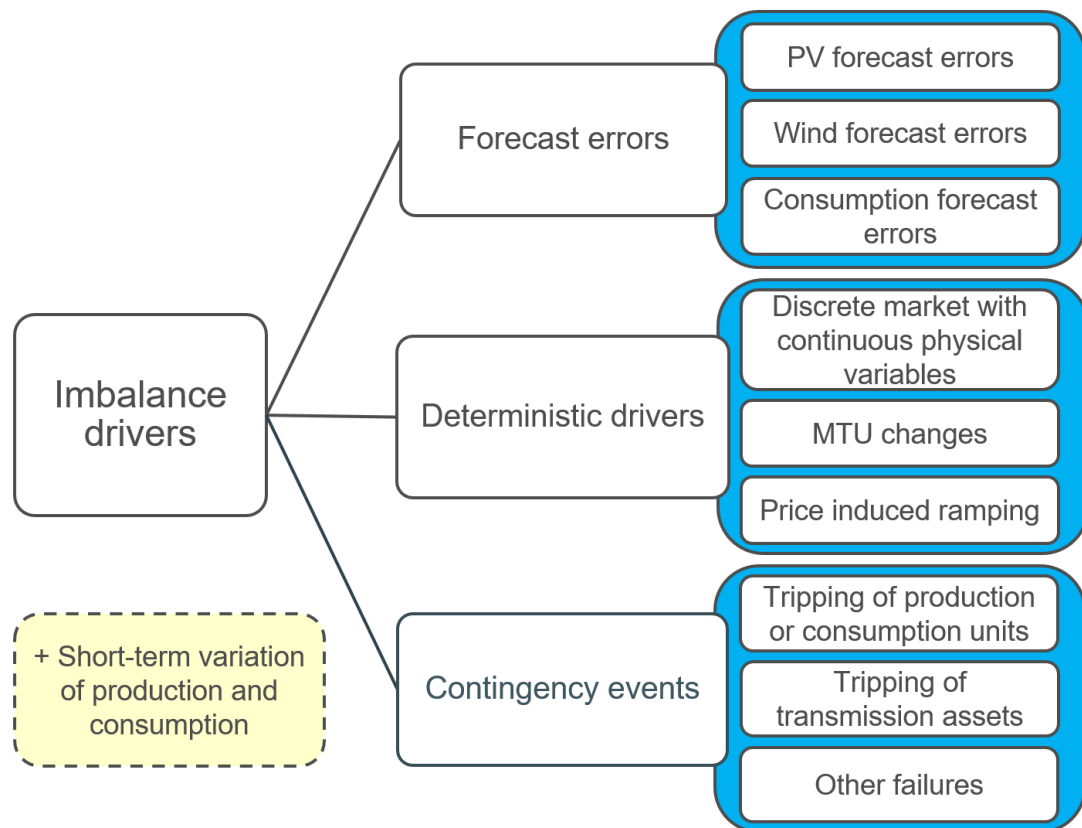


Figure 1: Overview of the different imbalance drivers and their causes, adapted from [2].

2.3.1 Forecast errors

As told earlier, the BRPs are expected to plan and control their electricity procurements and deliveries in a way that the realized imbalances stay on a reasonable level. This position management is largely based on the forecasts of consumption and intermittent renewable generation [2]. For this reason, forecast errors will lead to real-time balancing needs if they are not canceled out by opposite imbalances or corrected by the actions of BRPs.

The forecast errors themselves depend naturally on quality of used forecast models, and length of forecast horizon [25]. In addition to these factors, especially the renewable production forecasts are affected by the internal characteristics of the predicted variables [27][28]. Therefore, wind and PV production are overviewed with more detail from the predictability point of view in this sub-section. The choice of analyzing only wind and PV forecasts is due to their current or predicted dominance in the field of renewable generation inside the Nordic synchronous area [7].

While wind turbines are operating under their nominal power, their power output is related to the cubic of wind speed [29]. This in turn will lead to power variations with the changing wind speeds, as the turbine tries to extract the maximum power available from the wind. After wind speed has increased enough and the turbine reaches its nominal power, the variability of power output decreases as the turbine control starts to limit the mechanical power extracted from the wind. Due to this cubic relation and stabilization of power output after reaching nominal power, the forecast errors tend to be largest during mid-range production [28].

However, if turbine's cut-out wind speed is reached, the turbine is forced to shut down due to increased engineering loads and safety constraints [29]. For this reason, the likelihood of extreme forecast errors increases during storm events [30]. Extreme forecast errors are also likely to occur, if the timing of weather fronts with large wind speed changes are miss forecasted [31]. In contrary to factors reducing the forecast accuracy, the quality of forecasts is improved as multiple units from large geographical area are aggregated together [25]. Consequently, the predictability of dispersed onshore wind power tends to be better than the more concentrated offshore wind power [2][30].

The variability of PV systems' output power can be divided into deterministic and stochastic part [27]. Firstly, as the production of PV systems is dependent on the global irradiance reaching the plane of the PV array, the movement between Sun and Earth will induce a deterministic component into production variation. From the predictability point of view, the second component caused by stochastic behavior of atmosphere, is more challenging. Of the atmospheric phenomena, cloudiness and cloud movement are the most influential variables in terms of predictability [32][33]. Fortunately, also the PV forecast accuracy benefits from the aggregation of multiple units dispersed in large geographic area [34]. It is also good to note that while forecasted PV or wind production is close to zero, the forecast errors may only lead to underestimation of production [2].

2.3.2 Deterministic imbalances

Deterministic imbalances arise from the differences between discrete market schedules and continuous physical variables [26]. The first mechanism for the creation of deterministic imbalances relates to the inability of market resolution to describe the sub-hourly variation of production and consumption [35]. In practice, the BRPs could be perfectly in balance on the ISP level, even though their production or consumption varied significantly within the settlement period. The second mechanism is related to MTU shifts and merges as the ramping behavior of the production, consumption and High-Voltage Direct Current (HVDC) interconnections differs from each other [36].

The severity of deterministic imbalances depends largely on the length of the MTU and the ISP [35][36]. In practice, shorter ISP will create a financial incentive for the BRPs to balance their portfolios more accurately on an intra-hour level [35]. When the BRPs consider trading their projected imbalances away more beneficial than facing the costs of sub-hourly imbalance settlement, the resulting market schedules will follow the physical variables more accurately and tend to have lower changes between the consecutive market periods. First of these consequences affects directly to the deterministic imbalances arising from the non-descriptive market resolution. The lower amount of total ramped power will in turn lead to reduced mismatch between the ramping of production, demand and HVDC interconnections and thus diminish the deterministic imbalances during the MTU shifts [36].

Although price-induced ramping of renewable production is not directly related to either of the mechanisms presented in the first paragraph, it can be classified as a deterministic imbalance source. In the simplest form of price-induced ramping, production is ramped down between market periods in which the day-ahead market price changes from positive to negative and ramped up while the change of price is in the opposite direction [37]. Unfortunately, the imbalances caused by price-induced ramping are not affected directly by the shorter ISP. It is also good to note that since the wind and PV producers may have different thresholds for the profitability of generation, it is very challenging to predict how the producers will actually behave during the changes between positive and negative day-ahead prices.

2.3.3 Short-term variability

The short-term variation of consumption is caused by the stochastic behavior of consumers. The production's short-term fluctuation, on the other hand, is caused mainly by the

variability of renewable generation. In the Nordic synchronous area, this means practically the variation of wind and PV production as they are the dominant intermittent renewable energy resources in the area [7].

Of the relevant renewable production, the PV fluctuations tend to be faster than the wind power fluctuations [38]. The difference is caused by the PV's sensitivity towards fast irradiance changes, which are related to shadowing induced by cloud movement [33]. These irradiance changes will in turn directly affect the output power of the PV plant because it lacks a mechanical buffer between the source of energy and the produced power. Fortunately, the previously discussed smoothing effect due to the aggregation of wind and PV production is also present with the short-term variability [39].

2.3.4 Contingency events

Contingency events are imbalances created by unexpected outages of generation, demand or transmission assets [2]. Also, the busbar failures leading to tripping of multiple consumption or production units are a source of contingency induced imbalances [1]. The magnitude and direction of these imbalances are highly dependent on the prevailing system conditions [2]. For example, the level of HVDC export or maintenance schedules of production units affects understandably the properties of possible imbalances.

Largest generation outage risks in the Nordic system are related to the tripping of nuclear power plants like Olkiluoto 3, which impact to the system is 1300 MW in the case of full power trip [1][40]. From the demand side, the largest risks are associated to industrial consumption such as aluminum smelter halls [1]. In the case of transmission assets, tripping of HVDC interconnection or power lines combined with activation of system protection scheme create the main imbalance risks. To give an example, tripping of Nord-Link HVDC connection could lead to imbalances up to 1400 MW [41].

2.4 Balancing the power system in real-time

In addition to placing the TSOs as responsible parties for the real-time balancing, the SOGL sets boundaries for the implementation of balancing process itself [3]. Practically, it obligates TSOs of each synchronous area to specify a load-frequency control structure with the synchronous area operation agreement. In the Nordics, this treaty is called Nordic System Operation Agreement (SOA) [4].

This contract shall include process activation and process responsibility structures [3]. The process activation structure defines both mandatory and optional control processes, which are implemented and operated by the TSOs inside the synchronous area [42]. The

mandatory control processes defined by the SOGL are Frequency Containment Process (FCP) and Frequency Restoration Process (FRP) [3]. The process responsibility structure, on the other hand, defines the operation and control responsibilities in terms of geographical areas and TSOs [42].

The process activation structure is presented more accurately in the last two sub-sections of this chapter because it classifies the individual steps from the occurrence of frequency deviation to the recovery of nominal frequency [3]. However, the first sub-section of this chapter is reserved for the frequency quality defining parameters as they form a foundation for the actual control processes [43]. Before proceeding with the introductions, an overview of the control processes and their relation to actual reserve products is given in Figure 2.

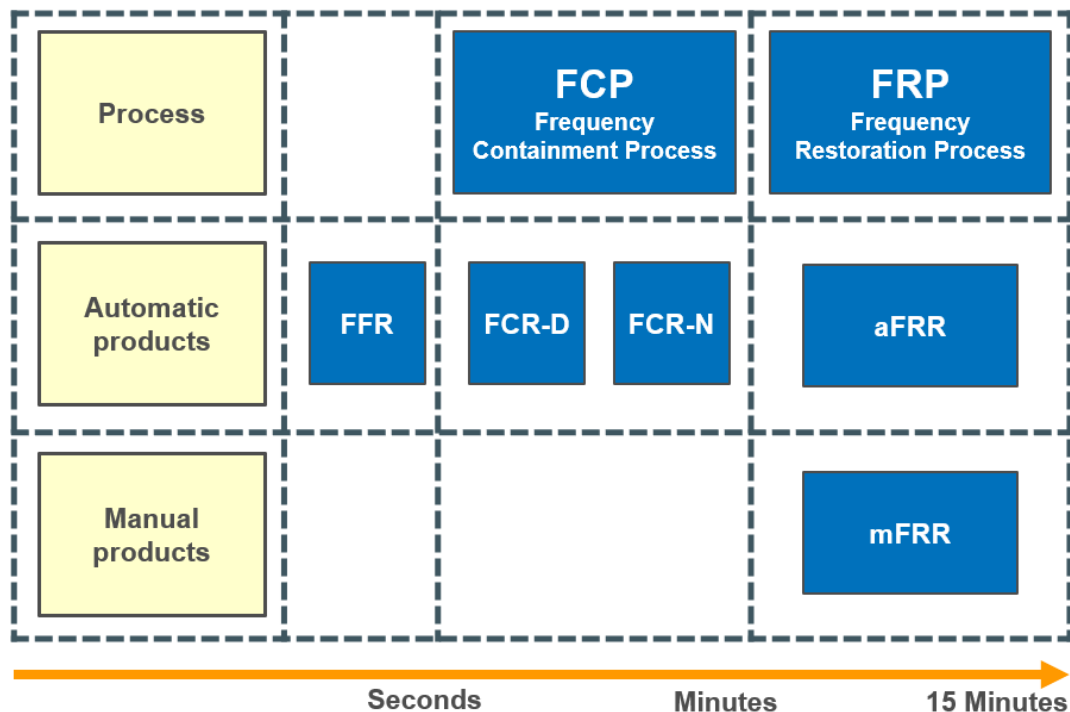


Figure 2: Overview of the reserve products in contrast to their activation times, processes in which they relate and control mechanisms, adapted from [5].

The x-axis of Figure 2 presents the activation times of different reserve products, corresponding to versatile timescales of system imbalances. Figure 2 also illustrates in which control process a certain reserve product belongs to and whether it is controlled manually or automatically.

2.4.1 Frequency quality defining parameters

According to the SOGL Article 152, each TSO should operate its control area with sufficient amount of active power reserve to reach the defined frequency quality targets within

the synchronous area [3]. By maintaining the frequency quality, the TSOs are also maintaining the power balance inside the synchronous area and accordingly a good security of supply level [43]. The frequency quality itself is defined with the help of frequency quality defining parameters [3]. Due to this connection, these parameters will also create a framework for designing the control processes and perform reserve sizing [43].

In practice these parameters define the acceptable frequency ranges, in which the frequency must stay during normal operation and after a reference incident without applying emergency measures [43]. In the Nordic synchronous area, the reference incident is defined to be the largest imbalance that may result from a single fault [44]. To give an example, reference incident can be a tripping of nuclear power plant or HVDC connection. Figure 3 demonstrates the frequency quality defining parameters relevant for the scope of this work.

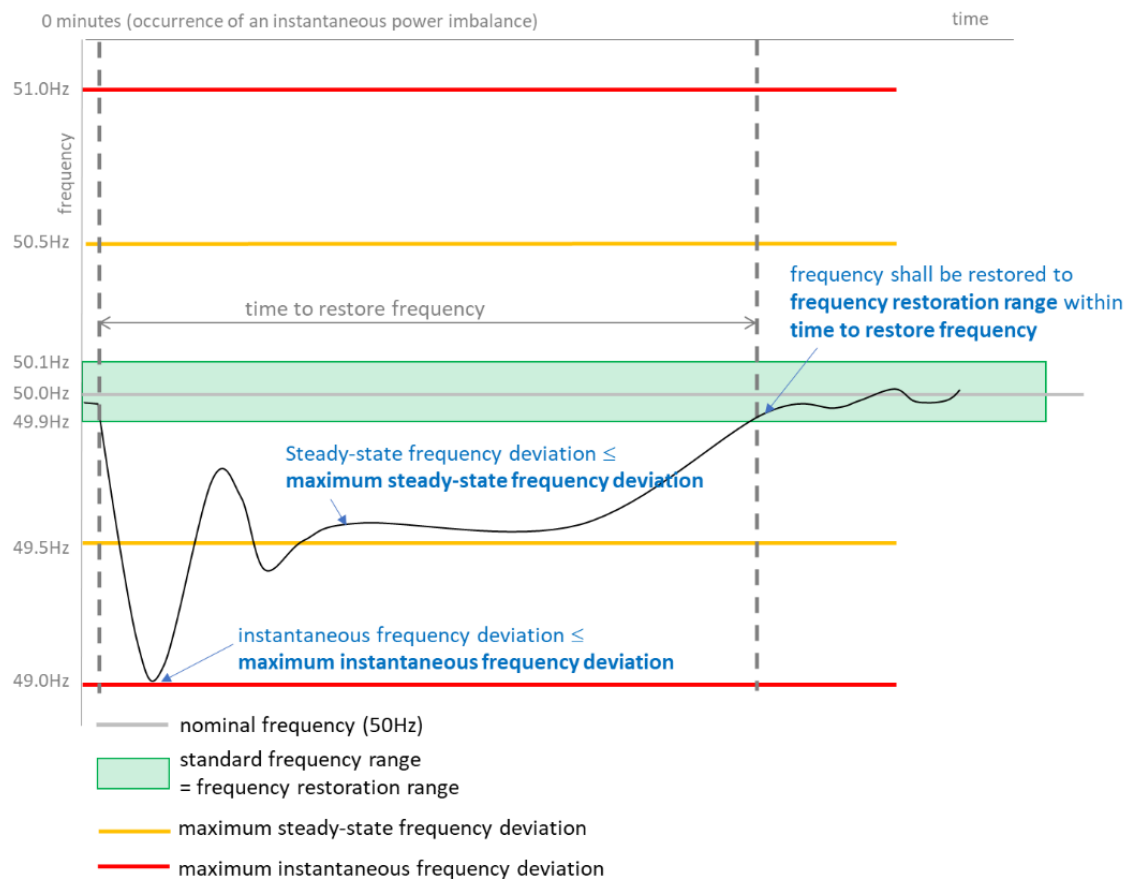


Figure 3: Frequency quality defining parameters applied in the Nordic synchronous area [43].

The *nominal frequency* forms a baseline for the other frequency quality defining parameters and it is defined to be 50 Hz in the Nordic synchronous area [3]. The second fundamental parameter is the *standard frequency range*, which corresponds to frequency

band of ± 100 mHz around the nominal frequency [45]. It is crucial that the frequency stays inside this range during normal operation to guarantee a large enough buffer for disturbances [43].

If the frequency exceeds this range during normal operation, the risk that the designed control processes are insufficient to cover the reference incident grows, as they assume that the frequency is inside this range before the occurrence of reference incident [42]. This range is also linked to the frequency quality target parameter defined by the SOGL, which is the maximum number of minutes outside the standard frequency range [3]. According to the SOGL the limit for this parameter is 15 000 minutes per year, but the Nordic TSOs have agreed to aim for 10 000 minutes [45].

Because of technical constraints, the operation of turbo generators is limited to a specific frequency range [43]. Thus, frequency deviations exceeding this range will lead to automatic disconnection of these generators due to the triggering of their protection mechanisms. This would in turn lead to major power deficit inside the synchronous area, as the generators experience the same frequency. In accordance with this limitation, the SOGL defines the *maximum instantaneous frequency deviation*, which sets a limit for the expected frequency value after the occurrence of imbalance with a magnitude up to the reference incident [3]. This parameter is defined to be 1000 mHz in the Nordic synchronous area [45]. It also sets a boundary for the activation of emergency measures, as the Low Frequency Demand Disconnection (LFDD) process starts to disconnect consumption after the frequency has decreased 200 mHz below this threshold [1][3].

The *maximum steady-state frequency deviation* is set to be 500 mHz from the nominal frequency and it defines the frequency range in which the system frequency must stabilize after occurrence of imbalance [3][45]. The *time to restore frequency*, on the other hand, refers to the maximum expected time following reference incident in which the frequency is returned inside the *frequency restoration range* [43]. In the Nordics, this time is defined to be 15 minutes [45]. The frequency restoration range refers now to frequency band in which the synchronous area is able to handle another reference incident without utilizing emergency measures, making it equal to the definition standard frequency range [43].

2.4.2 Frequency containment process

The first objective of the Frequency Containment Process is to cease the frequency deviation before it proceeds the limit of maximum instantaneous frequency deviation [42].

After ceasing the deviation, the FCP should stabilize the frequency inside the range defined by the maximum steady-state frequency deviation. The reserve products used for the FCP in the Nordic countries are Frequency Containment Reserve - Normal (FCR-N) and Frequency Containment Reserve - Disturbance (FCR-D). Also, Fast Frequency Reserve (FFR) is utilized to support the containment process occasionally. Before proceeding to a more detailed introduction of these products, the relationship between the activation of FFR, FCR and FRR is presented in Figure 4.

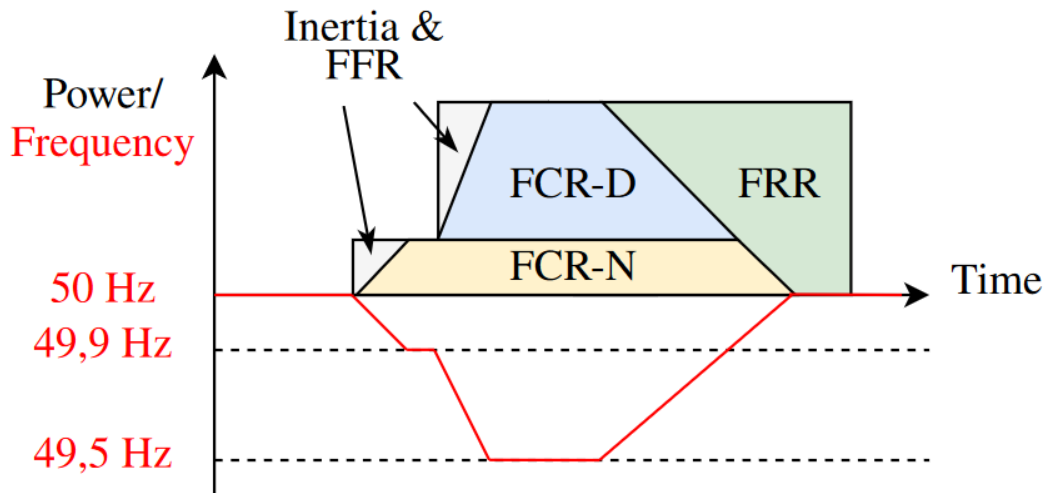


Figure 4: The activation of FFR, FCR and FRR reserves in the case of frequency deviation [46].

The role of FCR-N is to maintain frequency stability within the standard frequency range [42]. It is activated linearly according to the system frequency and its steady-state activation should reach 100 % of the maintained capacity with frequency deviations equal to or larger than ± 100 mHz [1][47]. It is also a symmetrical product and thus the reserve providing entities maintaining FCR-N must have the capability to increase or decrease their power exchange with the grid, according to the direction of frequency deviation [1].

The FCR-D, on the other hand, is used to mitigate the impact of contingency events, which are causing frequency deviations exceeding the standard frequency range [42]. As the activation of FCR-D starts after frequency drops under 49.9 Hz or rises above 50.1 Hz, it is implemented as two individual products: FCR-D upwards and FCR-D downwards [1]. The activation of these products is also proportional to the frequency and their steady-state activation should attain 100 % of the maintained capacity, if the system frequency reaches 49.5 Hz or 50.5 Hz [47].

The requirements considering the dynamic behavior of FCR products are defined in a joint Nordic technical requirement document [47]. According to this document, reserve units maintaining FCR-N should activate approximately 63 % of the final value in 60

seconds and around 95 % in 3 minutes after a step change of ± 100 mHz from the nominal frequency [48]. As the FCR-D is utilized in the case of contingency events, it has stricter dynamic performance requirements than the FCR-N [47]. These requirements are defined, in conjunction with the frequency ramps of ± 0.24 Hz/s from 49.9 Hz to 49.0 Hz (FCR-D upwards) or from 50.1 Hz to 51 Hz (FCR-D downwards), by Equations 3 and 4:

$$|\Delta P_{7.5s}| \geq 0.86 \cdot |\Delta P_{ss}| \quad (3)$$

$$|E_{7.5s}| \geq 3.2 \text{ s} \cdot |\Delta P_{ss}|. \quad (4)$$

In the equations above, $\Delta P_{7.5s}$ (MW) refers to the activated power 7.5 seconds after the start of the frequency ramp, ΔP_{ss} denotes the calculated steady-state response in MW to the frequency change of ± 0.4 Hz exceeding the threshold of FCR-D activation and $E_{7.5s}$ means the activated energy in MWs from the start of the frequency ramp to 7.5 seconds after the start of the ramp [47].

During the times FCR-D would be insufficient to stabilize the frequency before exceeding the maximum instantaneous frequency deviation, FFR is utilized to support the frequency containment process [42]. In practice, these conditions are fulfilled when the system inertia is low, and the reference incident is large enough. The activation of FFR starts as the frequency crosses the activation threshold value which can be some of the following: 49.7 Hz, 49.6 Hz or 49.5 Hz. The acceptable time to reach full activation is in turn linked to these threshold values, but it is not more than 1.3 seconds.

In the Nordic synchronous area, the dimensioning of the FCR-N is currently built on historic assumptions of random load variation, which leads to securing 600 MW of FCR-N annually in both up and down direction [1]. The volume of the procured FCR-D, in turn, is based on a common Nordic reference incident. Since the need of FFR is based on the system inertia which varies according to production and consumption, the amount of procured FFR is also dynamic. Practically, the needed FFR capacity is evaluated by using inertia forecasts and simulating valid reference incidents for the target day.

The responsibility of maintaining sufficient amount of FCR-N and FCR-D is divided between the Nordic TSOs according to the annual net production and consumption inside each TSOs' control area [1]. The sharing of FFR responsibility is in turn agreed annually by the Nordic TSOs, but it resembles the sharing key of FCR [1][42]. The procurement of these reserves is currently done through national capacity markets [1]. In addition to local markets, part of the TSOs obligation may be fulfilled through exchange of reserve capacity. In practice, the exchange of capacity means that one TSO may buy additional capacity from its national market and sell it to another TSO.

2.4.3 Frequency restoration process

In the Nordic synchronous area, the aim of Frequency Restoration Process is to restore the frequency back to its nominal value [3]. This process will also replace the activation of the FCR reserves, freeing them to be ready for the occurrence of next system imbalance [1]. On a product level, the Nordic FRP is based on aFRR and mFRR reserves [42].

The FRR products cannot be classified as clearly according to their basic function as in the case of FCR products, since both aFRR and mFRR are used for restoring the frequency [1]. Indeed, the differences between these reserve products are related to their control implementation and dynamic behavior [1][42]. While reading this chapter it is good to note that the Nordic balancing process is currently undergoing major changes and thus many of the details introduced in this chapter will be outdated in the near future [49]. The future implementation of FRP is presented in sub-section 3.3 of this thesis.

As the name suggests, mFRR is activated manually according to the TSOs' needs [1]. The full activation time of mFRR bid is 15 minutes from the TSO's request and this activation can be based on realized or expected imbalances. In addition to balancing purposes, mFRR can be used for special regulations [5]. One practical example of these special regulations is to use mFRR activations in the congestion management of the transmission grid.

The aFRR is in turn activated centrally by a single Load-Frequency Controller (LFC), which calculates the needed activation based on the system frequency [42]. This activation request is distributed to the Nordic TSOs pro-rata, after which each TSO redistributes it to the BSPs maintaining aFRR inside its control area. The full activation time of aFRR is at most 5 minutes, making it a faster product than mFRR [1].

Currently mFRR is dimensioned to cover at least the reference incident of each control area [42]. The dimensioning of mFRR is done according to the national reference incident, since grid congestions may restrict the use of mFRR activation from one area to cancel the imbalance in another control area [1]. The volume of procured aFRR is in turn based on frequency quality targets and it is maintained during hours in which the frequency deviations are most challenging [42]. For the hours in which aFRR is procured, the minimum value is defined to be 300 MW in the Nordic level [1]. The sharing of aFRR responsibility is defined on an agreement made by the Nordic TSOs, but as in the case of FFR, also it resembles the sharing key of FCR.

The procurement of mFRR is done through common Nordic energy activation market, in which the bids of Nordic BSPs are gathered [1]. During operation, these bids are activated according to the system needs and if no grid congestions arise, these activations

are done in a price order. In Finland, the procurement of aFRR is also done through energy activation market and the activation order of these energy bids is similar to the mFRR market [50].

To fulfill the dimensioned volume of FRR, there is currently a common Nordic capacity market for the aFRR and national markets for the mFRR [1][49]. If BSPs' bids are accepted on these markets, they are obligated to offer at least corresponding volume to the related energy market [50][51]. In those Nordic countries, where aFRR energy market is not yet implemented, the capacity market defines also the BSPs which will activate the aFRR during operation [50].

3. FUTURE POWER SYSTEM

On a general level, estimating the balancing needs of future power system is based on two factors. Firstly, one must understand the imbalance creation mechanisms themselves. Secondly there must be an awareness of the future developments affecting the balancing needs. As the imbalance drivers were already discussed in section 2.3, the first three sub-sections of this chapter will concentrate on the upcoming changes in power system, electricity markets and balancing.

After this future development outlook, the fourth sub-section will give a brief overview of the methodologies used in the recent balancing need and dynamic reserve dimensioning studies. Finally, before proceeding to the empirical part of this thesis, the last section will define the cases which are further investigated in this work. These cases are based on the projected development presented earlier in this chapter and the results of previous balancing need outlooks.

3.1 Changes in production and consumption

To reach the climate neutrality aim of the European Union by the year 2050, the transport, energy and industrial sectors must be renovated in Europe during the next decades [7][8]. The electrification of these sectors can be seen as one of the key measures to execute this transformation [7]. This will in turn lead to a significant increase in demand of electricity. In addition to the electrification of these sectors, it is predicted that demand will grow due to rising energy intensive industries such as battery and green hydrogen production and commercial activities like data centers. Based on this projected increase of demand, fossil-free electricity production is also expected to grow considerably in the coming years.

The predicted developments presented in this chapter are mainly based on Fingrid's own estimate: *Prospects for future electricity production and consumption* [52]. This forecast is based on the results of electricity market modeling and connection agreements and enquiries considering production, storage and consumption projects. As the market modeling considers also the Baltic Sea region and central and western Europe, the development of these areas is estimated by using corresponding TSOs' forecasts and scenarios made by the European Network of Transmission System Operators for Electricity (ENTSO-E). The reason for concentrating mainly in Finland's projected development, is due

to the scope of this work and the more localized nature of future balancing process, which will be described with more detail in sub-section 3.3.

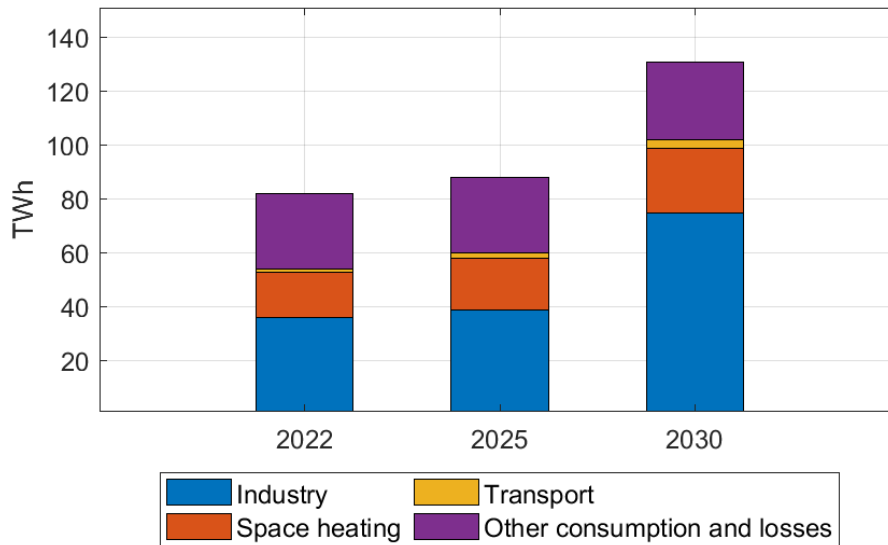


Figure 5: Predicted development of electricity consumption in Finland, adapted from [52].

As seen from Figure 5, industrial electricity consumption forms the largest driver for expected growth [52]. Although the previous figure is presenting the situation in Finland, similar development is also expected for other Nordic countries [7]. Roughly half of this increase is due to hydrogen and electric fuel production [52]. Rest of the predicted industrial growth is created by activities such as electrical metal processing and electrical heat and steam production. Besides industrial growth, the electrical space heating and especially the electrification of district heating is expected to be a major driver for the electricity demand.

The forecasted increase in electrical use of transportation is based on assumption of 800 000 to 900 000 electric and plug-in hybrid passenger cars by the year 2030 [52]. The range in the number of cars is due to consumption's dependency on the mileage and specific consumption. In addition to the passenger cars, the presented number includes the direct electricity use of heavy-duty and railway transport [53]. Although the impact of electrical transportation is predicted to be relatively low on an annual level, it will impact the need of momentary electrical power through high-power charging of electrical cars [52]. It is also noteworthy that this number excludes the electricity fuel production for transportation usage, as it was already included in the industrial growth.

On the production side, wind and solar power are expected to be the largest growth factors in the Nordic area [7]. Other fossil-free technologies are expected to stay rela-

tively constant in coming years, as for example most of the hydro power suitable locations are already in use. These trends are also valid in the case of Finland, which can be seen from Figure 6 below [52].

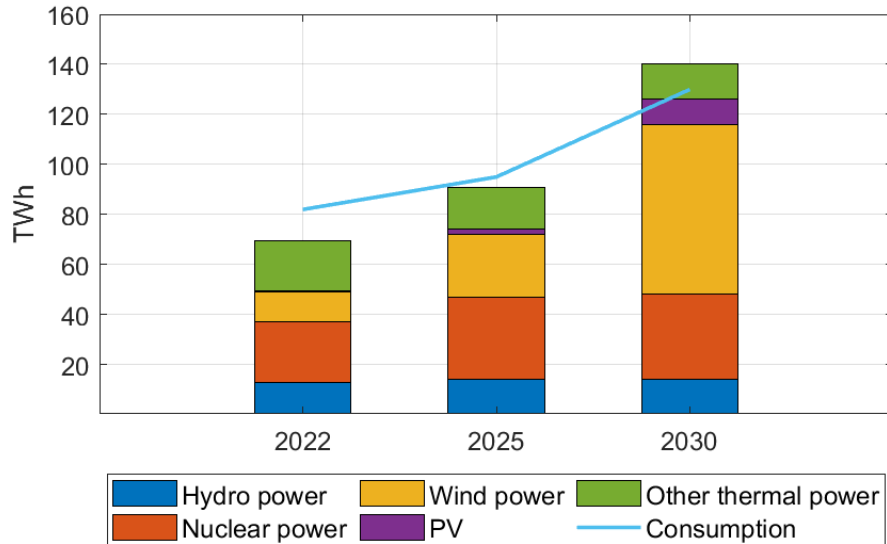


Figure 6: Predicted development of electricity production in Finland, adapted from [52].

Wind power is predicted to be the largest source for the production growth in Finland [52]. Most of this growth is due to onshore wind power, as it is predicted that the rise of large-scale offshore wind power will not begin until the early 2030s. Although in past few years, the solar power capacity has increased mainly due to installation of rooftop solar panels, the predicted increase in Figure 6 is created mainly by the large-scale solar farms.

Nuclear power production capacity is expected to increase slightly as a resultant of designed power upgrades to Olkiluoto 1 and 2 power plant units [52][54]. Rest of the thermal power production is expected to decrease somewhat due to the closure of fossil power plants [52]. The hydropower capacity, which is now excluding the production of pumped storage power plants, is estimated to stay close to current levels.

Before proceeding to the next part of this chapter, the reader is reminded that the expected development presented in this section includes many uncertainties. The predicted evolution of production and consumption is dependent on factors such as project financing, energy policy, regulation and cost development of hydrogen technologies [52]. The link between these factors and the total forecast uncertainty can be explained by the causality between cheap and clean electricity production and realization consumption projects.

3.2 Electricity market changes

First of the market changes affecting the balancing needs, is the Nordic transition from standard market time unit of 60 minutes to 15 minutes in both day-ahead and intraday markets [24][55]. The basic idea behind shorter MTU is to enable trading which describes the physical behavior of variable production and consumption more accurately [55]. In other words, finer market resolution will give an additional tool for the BRPs to balance their portfolios on a sub-hourly level. This will in turn diminish the balancing needs arising from the deterministic imbalances, when the BRPs actively utilize the possibility to trade with finer resolution [35][36].

The Nordic implementation of 15-minute day-ahead and intraday markets is scheduled to go live in the beginning of 2025 [24]. The imbalance pricing will also change from the current 60-minute pricing to 15-minute imbalance pricing in accordance with these market reforms. This transition will make the imbalance pricing more presentative of actual imbalances, further increasing the financial incentive for the balancing.

As a second relevant market reform, the calculation of available transmission capacity given to the electricity market will be gradually changed from Net Transfer Capacity (NTC) based calculation to Flow-based calculation [24]. The goal of Flow-based methodology is to utilize the existing grid more efficiently from the overall economic benefit point of view compared to the NTC-based approach. In Finland, the market simulations have indicated that the Flow-based methodology will increase both the utilization rate of the existing transmission grid, and the amount of electricity exported.

Based on these projections, it is likely that the possibility to activate FRR from neighboring control areas for Finnish needs or net imbalances between different areas is changed after the implementation of Flow-based methodology. The first step of this reform will happen in October 2024, as the methodology is taken into use on the day-ahead markets [24]. The implementation of intraday markets and mFRR energy activation market will follow later, although the NTC of these markets will be derived from the results of day-ahead Flow-based calculation, already in October 2024.

Although not a market reform, the increase of cross-border transmission capacity due to the commission of Aurora line in 2025, must be highlighted in this sub-section for the same reasons as the Flow-based methodology [56]. Aurora line will increase the capacity between Finland and Sweden by close to 900 MW in the direction from Finland to Sweden. For the opposite direction, this change is around 800 MW.

3.3 Balancing of the future power system

The largest change in the balancing of the Nordic power system is the coming transition from frequency-based approach to Area Control Error (ACE) based balancing [55]. In the new balancing model, each load-frequency control area is balanced individually based on their calculated power imbalances, instead of using the frequency of whole synchronous area [1]. These areas correspond to the bidding zones in the Nordic system [42]. On a product level this transition will directly affect the implementation of mFRR and aFRR reserves [1]. Although the bidding zones are balanced individually in the new model, the Nordic implementation will utilize cross-zonal imbalance netting and reserve activations [55]. The idea of imbalance netting is to avoid opposite direction reserve activations, if the cross-zonal transmission capacity enables netting the balancing needs between different control areas [57][58].

To enable this transition, the Nordic TSOs have set up Nordic Balancing Model collaboration [49]. This program includes many individual projects, and its final goal is to enable the Nordic connection to European energy activation platforms: MARI (mFRR) and PICASSO (aFRR) [55]. Before connecting to the MARI platform in 2026, there will be automated Nordic mFRR Energy Activation Market (EAM) [49]. The automated mFRR EAM is scheduled to go live in December 2024 and it will act as a bridge between current manual process and fully automated MARI platform [49][59]. Also, the onboarding to PICASSO platform will happen in steps, as Finland and Denmark will access the platform in October 2024 and rest of the Nordic countries will follow in 2026 [49].

In addition to the energy markets reforms, also the FRR capacity markets will experience changes, as the common Nordic mFRR capacity market will be launched between 2025 and 2026 [49]. To make procuring of FRR capacity across the bidding zones possible, there will be an option to allocate part of the cross-zonal capacity for FRR usage before sending it to the NEMOs [60]. The amount of allocated capacity is based on the forecasted socio-economic benefit of reserving cross-zonal capacity for balancing purposes instead of giving it to the electricity markets. This capacity reservation can be up to 10 % in one bidding zone border, and in the case of scarcity this percentage can be raised up to 20 %. From the FRR products, aFRR has the priority to access this allocated capacity, and thus the mFRR capacity market can utilize only the remaining part of the allocated capacity which is not used by the aFRR capacity market.

After the go live of automated Nordic mFRR EAM, the activation of mFRR will be based on forecasted imbalances of each bidding zone, changing the control philosophy from

mainly reactive to preventive control [59]. These forecasted imbalances are sent to Activation Optimization Function (AOF), which will determine the best available bids placed on the mFRR energy market to balance the system, while taking into account the available transmission capacity and the price of the bids [1][59]. After this optimization process, the TSOs will make bidding zone specific mFRR activation request based on the results of the AOF [61]. This cycle will be repeated on every 15 minutes. Besides to the scheduled activations due to forecasted imbalances, both the Nordic mFRR EAM and the latter MARI platform will allow direct activations which are done to compensate unexpected imbalances [57][62].

Although Finland and Denmark will onboard the PICASSO platform already in 2024, the activation of aFRR continues to be based on the centralized controller [50]. This will be changed with the Nordic PICASSO accession in 2026 [49][50]. After the common onboarding, each bidding zone will have their own load-frequency controller, which will regulate the power balance inside the corresponding area [50][61]. This controller will also utilize AOF to optimize the activation of aFRR energy bids, in order to efficiently use the available transmission capacity and the placed offers [61].

In a more practical level, the LFC aims to regulate the Frequency Restoration Control Error (FRCE) of each bidding zone to zero [58]. The FRCE is calculated by Equation 5:

$$FRCE = \Delta P + K\Delta f, \quad (5)$$

where ΔP denotes the difference between scheduled and measured power exchange between the bidding zones and $K\Delta f$ is correction term taking into account the self-regulation of load and the activation of frequency containment reserves [3]. The correction term is calculated from the product of bidding zone specific K -factor (MW/Hz) and measured frequency deviation Δf . While driving the FRCE of each bidding zone to zero, the aFRR will replace the activated frequency containment reserves and return the cross-zonal exchange to scheduled values [58]. This will in turn lead to retaining the nominal frequency inside the synchronous area. As the PICASSO platform enables cross-zonal aFRR activations, the actual input of Finnish LFC is corrected by the amount of aFRR which is activated on behalf of Finland in other areas (or vice versa) [46].

The reforms explained in this sub-section will make the balancing process more localized compared to the current frequency-based approach, since each bidding zone will be controlled individually. On the other hand, the balancing needs themselves will be more dynamic in the future, as for example the imbalances arising from forecast errors are

more likely during windy periods than calm days [10]. For these reasons, also the dimensioning principle of mFRR and aFRR will be reformed after the launch of Nordic PICASSO [63].

In the renewed methodology, the aFRR and mFRR are dimensioned jointly by considering the balancing needs arising from both contingency events and normal imbalances [63]. The normal imbalances are defined in this methodology as imbalances created by drivers such as forecast errors and stochastic load variation. According to this methodology, the mFRR is dimensioned to cover at least the reference incident of each control area and part of the normal imbalances, while the aFRR is dimensioned solely for the latter. The division between aFRR and mFRR with normal imbalances is based on the activation times of these products. As the new dimensioning process will be ultimately repeated on a daily basis, it enables procuring more FRR during challenging conditions like windy periods and vice versa if the likelihood of imbalances is smaller [10][64].

3.4 A brief overview of methodologies used in recent balancing need and dynamic reserve dimensioning studies

The ongoing transformation in the electricity system has motivated many entities to perform integration studies which try to quantify and understand the balancing needs of the future power system [9][10][11]. Also, the dynamic dimensioning of reserves has gained a lot of attention recently, as it enables procuring reserves cost efficiently while maintaining defined reliability level [2][65][66]. Although the first of these study genres is interested in future development whereas the later one tries to support the daily system operation, the methodologies used in both study genres are quite similar. To lay groundwork for the thesis methodology selection, the following paragraphs will describe the main approaches used in the recent dimensioning and integration studies.

On a high level, the methodologies used in the reserve dimensioning and balancing need outlooks can be divided to deterministic and probabilistic approaches [67]. In the simplest form of deterministic methodology, the reserve requirements are derived from the linear sum of different possible events, which would lead to system imbalances when realized. To consider the lack of correlation between these uncertainty sources and avoid the overestimation of reserve needs, this approach can be improved by applying some form of geometric sum for the uncertainty factors or weighting the individual factors by defined percentage. The current mFRR dimensioning process is a practical example of the deterministic methodology usage, as the procured volume is based on the national reference incident [42].

The probabilistic methods, on the other hand, use often some specified reliability level to define the required reserve capacity from the estimated Probability Density Function (PDF) of the system imbalances [26]. The simplest probabilistic approaches use statistical parameters, such as standard deviation, to estimate the development in the reserve needs after some specified system change [2][67]. The shortcoming of this approach is the need to assume that the modeled uncertainty factors, related to both original and changed system, are normally distributed and uncorrelated [67]. In practice, for example the wind power forecast error distributions might be heavy tailed and skewed, which makes this assumption questionable [65].

The more complex probabilistic approaches model different uncertainty factors such as forecast errors and generator outages with probability density functions and combine these distributions into a single PDF, which will then express the probability of system level imbalances [67]. These individual uncertainty PDFs can be modeled either by using parametric distributions or kernel-based nonparametric methods [65][68]. To make this approach dynamic, the PDFs can be conditional in relation to different system conditions [2]. These conditional distributions are formed by dividing the history data expressing the uncertainty factors into subgroups according to specified system conditions, before creating the individual PDFs [65]. In practice this classification process can be done by using machine learning techniques such as k-means clustering. To give an example of this approach, there can be different PDFs expressing the uncertainty related to wind power forecasts for low, average and high production levels.

The combination process of individual PDFs itself can be done by using recursive convolution or Monte Carlo simulations [10][67]. In the convolution approach, individual PDFs are assumed to be statistically independent [67]. Also the combination process utilizing Monte Carlo simulations is bounded by this assumption if no additional steps are taken [69]. One possibility to consider the existence of correlation between different uncertainty factors is to use Cholesky decomposition with Monte Carlo simulations. Unfortunately, also this approach has its limitations as it naturally increases the computational work and is meant for normally distributed data.

Another limitation related to the methods using PDFs is their restricted ability to consider the changes in statistical characteristics of the uncertainty distributions while examining future scenarios [25]. For example, if historical wind power forecast error data is directly upscaled to investigate the development of balancing needs, this upscaling process assumes that the upcoming sites will be placed in the same locations as the current ones and the forecast accuracy will not improve in the future. This may in turn lead to overestimating the reserve needs as the approach is not considering implicitly the reduction in

relative forecasts errors due to increased geographical dispersion of production units or improved forecast tools [9][25].

Besides the methods explained above, there are machine learning techniques which can estimate the reserve needs without first forming PDFs for the individual uncertainty factors [2]. One popular approach within these methodologies is the use of neural networks. In practice, neural networks can be tuned to predict some specified quantile of system imbalance which will then directly define the needed reserve capacity. The downside of these approaches is their complexity and level of abstraction. The level of abstraction refers now to their limited ability to give information about the properties of uncertainty factors in different system conditions, as these methods forecast the balancing needs directly without first characterizing the uncertainty factors with PDFs.

3.5 Scenario building for the case study

The outlook of this thesis is built around four base cases in which the development of Finnish balancing needs is investigated. The first three cases are derived straight from the projected development presented in the previous sections and they correspond to years 2026, 2028 and 2030. The fourth base case presents the year 2033 and it is based on estimations made by Fingrid's specialists [70]. On a reserve product level, the examined balancing needs reflect the development of mFRR and aFRR requirements. To limit the scope of this work, balancing needs arising from contingency events and special regulations are excluded from the analysis. Also, the imbalance netting between the control areas is omitted during the case study, but its impact to the actual FRR procurement is discussed later in Chapter 6. The relevant estimated production and consumption values of the four base cases are summarized in Figure 7 below.

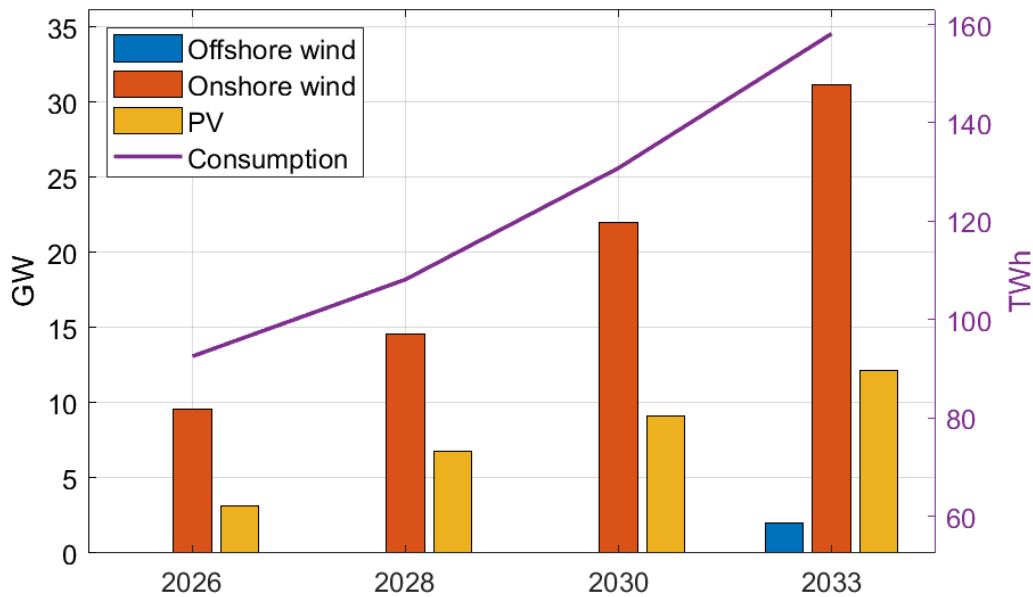


Figure 7: The production and consumption estimates related to the base cases in Finland [52][70]. The left y-axis of the figure is presenting installed capacity in GW and the right y-axis is presenting the yearly consumption in TWh. Note that the x-axis ticks are evenly spaced, although the years do not increase linearly.

The year 2026 is chosen to be the earliest year under examination, since all the balancing process and market reforms explained in sub-sections 3.2 and 3.3 are expected to be finalized before or during that year. Thus, all cases can use the same basic assumptions of the balancing process and market structure. The upper bound for the examined years is defined mainly by the increased uncertainty associated with further consumption and production development forecasts. The reason for including year 2033 as examined scenario while acknowledging its high forecast uncertainty, is due to the predicted rise of offshore wind power in the beginning of 2030 century [52]. Studying the effect of offshore wind power is considered important case because it has proven to be a significant driver of balancing needs in the previous outlooks [9][10].

To increase the robustness of the analysis, each base case is examined with different assumptions considering the market parties' ability to balance their portfolios closer to the delivery period as their production and consumption forecasts are updated. Also, assumptions related to the development of renewable production forecast accuracy are altered to model the effect of improving forecast models, increased geographical aggregation of forecast errors and possible self-balancing made by the market participants [65]. The self-balancing is defined in this work as real-time adjustments of production, demand or energy storage units in order to compensate the forecast errors [2].

As arbitrary iteration of market behavior and forecast accuracy would increase the computational workload significantly and lead to irrelevant combinations, three sub-scenarios are derived corresponding to conservative, moderate and advanced developments. The different assumptions considering these sub-scenarios are illustrated in Figure 8 below. The link between forecast horizon presented in the figure and the market behavior mentioned earlier will become clearer as the methodology of this thesis is explained in the next chapter.

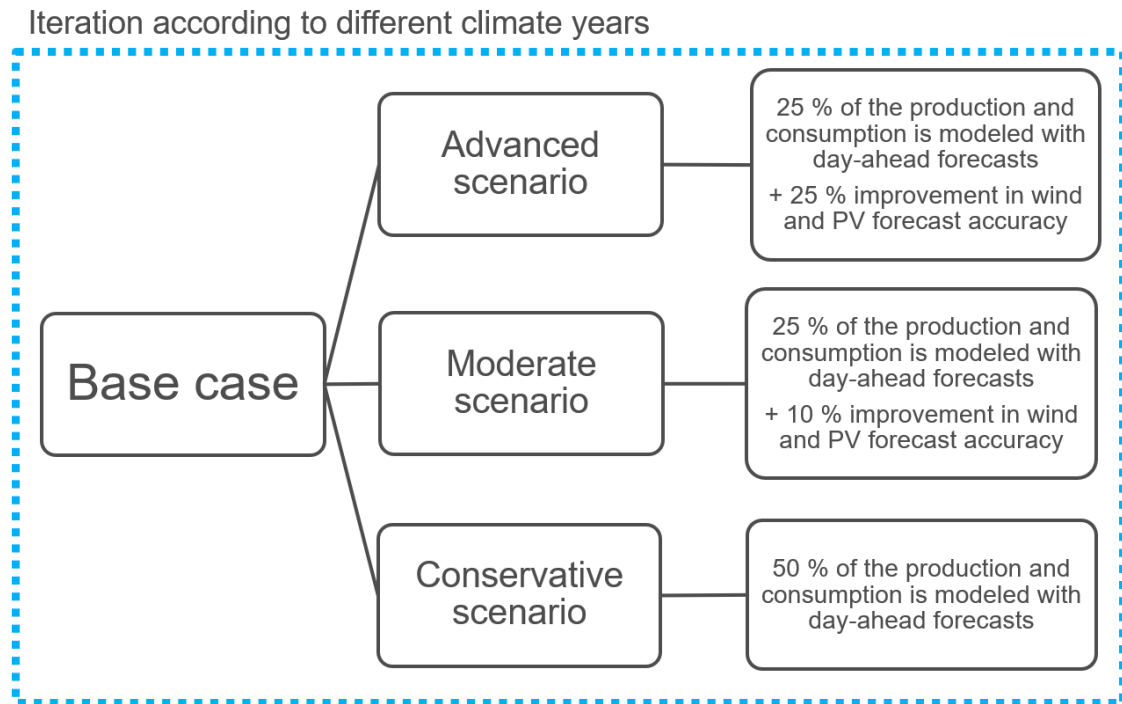


Figure 8: The different sub-scenarios within each base case. The properties presented in the right most boxes express the difference from a situation in which all forecasts used for the modeling process would have 1-hour prediction horizon.

Besides to already introduced variables, iteration according to different climate years is highlighted in Figure 8. The reason to use different climate years lies in the presupposition that weather-dependent production will be a major driver of balancing needs in the future and thus years with higher intermittent production levels are likely to correlate with higher balancing needs [10]. To keep the workload reasonable, the number of climate years analyzed in this work is also limited to three: high, mid, and low wind year. These years are defined from a set of available historical climate years [71], by first simulating electricity markets in the year 2026 with all available climate years, and then choosing the low, mid, and high wind scenarios according to the annual onshore wind generation. The market model used in this selection is discussed with more detail in sub-section 4.3.

4. METHODOLOGY FOR ESTIMATING THE DEVELOPMENT OF BALANCING NEEDS

From the methodologies overviewed in sub-section 3.4, the approach of this thesis is built upon probabilistic methodology utilizing conditional PDFs and it is derived from the approach used in [65]. The underlying reason for choosing this method is related to the insight it provides about the behavior of the uncertainty factors in different system conditions. On the other hand, it lines up quite well with the upcoming dynamic FRR dimensioning, in which the amount of total FRR is based on reliability level and historical imbalances [63]. The third criterion for choosing this methodology is the future's ACE-based balancing process, where local imbalances lead to local balancing needs if they cannot be netted out. Also, the level of complexity of this approach is seen appropriate for the scope of this thesis.

The added value of this work comes from the fact that there are no recent studies that have estimated the development of Finnish intra hour balancing needs with a resolution finer than a one year. On the other hand, this work uses different forecast horizons to model the behavior of market participants, which can be considered as a novel approach in the field of balancing need studies. The structure of the following sections resembles intentionally a process description since the used approach is highly dependent on representative history data and thus is beneficial to perform regularly.

4.1 Overview of the thesis approach

On a high level, the approach of this work can be divided into three phases. In the first phase, the aim is to estimate conditional PDFs for uncertainty factors that are creating balancing needs. In practice, distributions are created for the forecast errors related to wind power production, PV production and consumption. The forecast errors are defined in this work as a difference between ISP's measured and forecasted average power and they are calculated by using historical forecast and measurement data [72]. The formula used in this error calculation is presented below:

$$\epsilon_{i,t} = x_{i,t} - \hat{x}_{i,t}, \quad (6)$$

where $\epsilon_{i,t}$ denotes the calculated forecast error of forecast type i at quarter-hour t , $x_{i,t}$ refers to the measured average power and $\hat{x}_{i,t}$ is the forecasted average power. The "forecast errors" related to the difference between measured conventional, hydro, or nuclear power generation and their corresponding production plans are excluded from the

thesis analysis. This might be an optimistic assumption but can be justified by the 15-minute imbalance pricing and settlement period, incentivizing the BRPs to follow their production plans accurately.

The link between balancing needs and the forecast errors can be explained by the prediction horizon of the historical forecast data used in the creation of error PDFs. While using a one-hour prediction horizon, it is thought that the forecast error describes the realizable imbalance that remains after the market participants have tried their best to balance their portfolios, considering the information they have available an hour before the delivery period. In practice this corresponds to a situation in which the market participants are trading actively on the intraday markets. The use of day-ahead forecasts, on the other hand, models a situation in which the market participants only trade on the day-ahead markets and thus the day-ahead forecast errors can be seen as a realizable imbalance during the delivery period. Compared to the forecasts using one-hour horizon, the day-ahead forecasts are created once a day, close to 6 pm CET, by combining multiple forecasts with different forecast horizons [71][73]. The prediction horizons of the day-ahead forecasts used in this work vary between 6-29 hours.

In the second phase of the thesis approach, a market model is used to simulate the electricity market in the defined cases. As a result of this simulation process, hourly time series for production and consumption are created for each case. It is important to clear out that this work directly uses the market simulation results created by the Fingrid's specialists, even though running the market model is described as an individual phase of the thesis approach.

In the final phase, we select the PDFs created during the first phase that align with the market simulation results and form joint distributions by convolution. The joint PDFs are then used to determine the balancing needs by means of an attached reliability level. The reliability level used in this work is 97 % and it describes the probability that the amount of reserve capacity suggested by the thesis approach is sufficient to cover the balancing needs arising from the modeled uncertainty factors in conditions similar to those described by the outcome of the market model. The different phases of the used approach and their internal characteristics are illustrated in Figure 9.

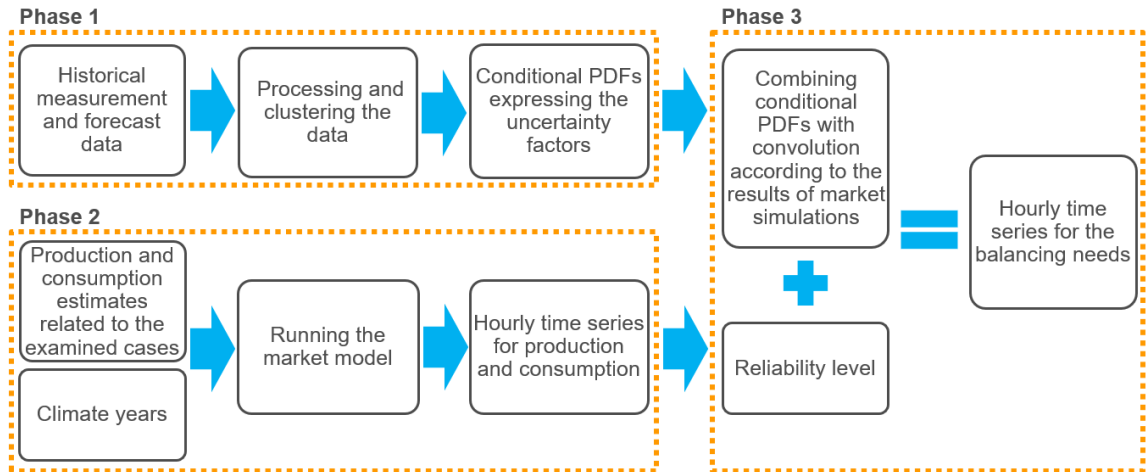


Figure 9: Overview of the thesis approach.

The connection of the balancing needs modeled by the forecast errors and individual reserve products can be explained by the mFRR bid activation profile [57][62]. After the go live date of automated Nordic mFRR EAM, the mFRR bids which are activated based on the forecasted imbalances, should ramp within ten minutes around the MTU chances and maintain their full activation for 5 minutes [62]. Thus, the activated mFRR bid or bids will theoretically compensate a forecast error equal to its combined peak power as their energy contents line up. However, as the activation request of mFRR is based on the forecasted imbalances, it cannot be always strictly equal to the actual mFRR demand. For this reason, part of the balancing needs estimated by the thesis methodology are practically compensated by the aFRR. Unfortunately, the split between aFRR and mFRR needs arising from forecast errors cannot be directly calculated, as it depends on the accuracy of forecast based mFRR activation requests and direct activation of mFRR.

Compared to the previous studies [66][72][74] utilizing similar approach, this work is not modeling the noise errors, as they cannot be directly combined with balancing needs in Finnish context. The noise errors arise from the short-term variation of production or load, and they are defined in the previous studies as a measured variation around the ISP's average power [66][72]. Although, the timescale of these variations resembles the activation time of FCR-N, they cannot be directly linked since the activation of FCR-N is based on the system frequency. In other words, national imbalances will not define the FCR-N activations, as the Nordic frequency is generated by the sum of imbalances inside the synchronous area.

Deterministic imbalances are also excluded from the modeling process, since they are expected to decrease after the implementation of 15-minute standard MTU and imbalance pricing. This restriction is also supported by the proposed HVDC interconnection

ramping restrictions and interpolation of the exchange schedules used in the load-frequency controller's FRCE calculation [46][75]. However, in order not to completely ignore the deterministic imbalances and to estimate the potential of price-induced ramping, Chapter 5 will briefly analyze the production and consumption changes between consecutive hours in the examined cases.

4.2 Phase 1: Data sources and processing

The historical forecast and measurement data considering onshore wind power and consumption is obtained from Fingrid's internal database [71]. The data for offshore wind power and PV production is in turn gained through Energinet's data catalog [76]. As Energinet's offshore wind power forecast data covers only wind parks with a capacity of over 100 MW and the available measurement time series includes all offshore wind parks, a forecast named *Forecast Current* is used to model the measured production [73][77]. The prediction horizon of this forecast is within a few minutes and thus it can be considered as a presentative time series for the real-time production [73].

Besides the historical measurement and forecast data, information about the installed wind and PV production capacity is needed to model the future balancing needs with conditional PDFs. This capacity data is used to transform the forecast errors to per unit values in relation to installed capacity. A similar scaling process is also executed for the consumption forecast errors, but historical hourly average peak demand of the related year is used instead of installed capacity. The following Equation 7 is illustrating the scaling process of forecast errors [65][66]:

$$\epsilon_{i,t}^{pu} = \epsilon_{i,t} \cdot \frac{1}{C_{SF}}, \quad (7)$$

where $\epsilon_{i,t}^{pu}$ denotes the per unit forecast error value and C_{SF} is a scaling factor corresponding to the installed capacity of the time in which the data was created or the peak demand of the related historical year.

As the PDFs are created later by using this scaled forecast error data, the obtained distributions can be adjusted to match the installed capacity or peak load of the examined scenarios. This adjustment process is executed at its simplest by sampling the per unit PDFs in a way that the number of samples between -1 and 1 is equal to desired capacity or peak demand in MW multiplied by two, plus one extra sample to consider the zero point of the PDFs' x-axis. To keep the integral of this new PDF equal to one, the sampled probability density values are divided by the related capacity or peak load in MW. In the case of offshore wind and PV, the required capacity data is obtained from the Danish

Energy Agency [78][79]. The capacity data considering onshore wind power is gained from Fingrid's open data platform [80].

In addition to the datasets discussed above, time series for mFRR down regulation prices and activations, day-ahead prices, and Global Horizontal clear sky Irradiation (GHlc) are required in the analysis. The usage of these datasets is explained with more detail in the following sub-sections, but in short, the regulation and day-ahead price data is used to filter undesired values from the forecast and measurement datasets while the GHlc data is used for clustering and choosing right distributions [65]. As the irradiation data is naturally dependent on the geographical location, city of Aarhus from Denmark and city of Jyväskylä from Finland are selected as reference points. This decision is justified by their central location compared to existing or planned PV installations [81][82]. The needed down-regulation time series are obtained through Energinet's data catalog and Fingrid's open data platform. The day-ahead price data is received from Nord Pool's data services [83]. Finally, the required GHlc data is generated by using Copernicus Atmosphere Monitoring Service [84].

By using the sources listed above, a database is created including values from the years 2021-2023. The decision to limit the size of the database to three years is due to the rapid pace of changes in the power system during recent years, making the older data no longer representative. It is also worth highlighting that the forecast data used in this work is created by the TSOs and thus it describes the system level production or consumption. This slightly differs from the premise of the thesis methodology, which builds on an idea that imbalances are created from the sum of the market participants' own forecast errors. Thus, the use of TSOs forecasts may disturb the modeling process as for example the forecast models used by the market actors may differ from the ones used by the TSOs.

Besides to the data used directly for the balancing need calculation, Finnish ACE Open Loop (ACE OL) time series is gathered from the period of 1.1.2023-30.6.2024. The ACE OL is defined as the real-time imbalance of a load-frequency control area before any balancing actions such as activation of FCR or FRR reserves [85]. This data is used later to optimize the number of clusters in sub-section 4.2.3 and benchmark the created balancing need calculation model in the beginning of Chapter 5. Since the analysis of this work is excluding balancing needs arising from the contingency events, frequency data is also gathered from the same period to exclude ACE OL values related to possible contingency events. The needed ACE OL data is obtained from Fingrid's internal database and the required frequency data from Fingrid's open data platform [71][80].

To use the ACE OL data for the predefined tasks, it must be augmented with Finnish PV, onshore wind power, consumption, and irradiation data. The required measurement and capacity time series for onshore wind power, consumption and irradiation are gained from the sources introduced above. The needed PV data is in turn obtained from Fin-grid's open data platform [80]. As there were no measurement time series available for the PV production, a forecast with quarter-hourly resolution and 15-minute lead time is used instead of real measurement data [86].

4.2.1 Data preprocessing

Before clustering the historical data and forming the conditional PDFs, the forecast and measurement data must be preprocessed. The first reason for this processing need is the mFRR down-regulations of wind and PV production, which would create fictitious errors while comparing the forecasted and measured data. As a result, datapoints generated during periods of down-regulation with negative prices are excluded from the production datasets. This processing need considers also the offshore wind power production as the used time series *Forecast Current* takes into account the possible down-regulation [87].

The negative prices are thought to be associated with situations where it is profitable for the wind or PV producers to participate in the down-regulation, as they can receive money by reducing their production [88]. However, it should be noted that this filtering method is not flawless due to the possible feed-in tariffs and various operational costs of the wind and PV producers [89]. This approach may also remove more datapoints than necessary because it does not account for whether wind or PV production is actually involved in the down-regulation.

Although similar distortion of the modeling process is present with the consumption data, it is not separately filtered out. The reason for this simplification lies in the increased complexity of the filtering as one cannot assume a more likely direction for the regulations or a certain price threshold after which the regulations would be profitable for the market actors. On the other hand, if all hours with mFRR regulations were removed, the amount of data would be significantly reduced without necessarily improving the overall modeling accuracy. It is also important to note that both FCR and aFRR activations can potentially disrupt the modeling process in similar ways but are not separately considered, to keep the complexity of the approach reasonable.

The second processing need relates to the negative day-ahead prices. This issue can occur if the wind or PV production forecast data is generated using prediction model that

does not consider the results of the day-ahead market. In practice, this distortion is created when some of the production bids placed on the day-ahead market are not accepted and the market participants are unable to sell this available production before the delivery. In other words, the market participants are incentivized by the settlement costs to operate below the maximum power point if there is no buyer for their production. This processing need mainly affects the onshore wind power data, as the day-ahead price was not added to the used forecast model until 2023, and the PV and offshore wind power forecasts consider the BRPs' production plans while making the predictions [87][90]. To eliminate this source of distortion, part of the datapoints related to times of negative day-ahead prices are removed from the onshore wind power time series.

The third processing need is induced by the mismatch in the resolutions of available and needed forecast data. The resolution of Fingrid's forecasts data is 1 hour and Energinet's 5 minutes, whereas the methodology of the thesis would require forecast data of 15-minute resolution. In the case of Energinet's data this problem is overcome simply by calculating the mean of three consecutive prediction periods and using it as a 15-minute resolution forecast. A similar approach is also used while estimating the measured offshore production with Energinet's forecast data.

In the case of Fingrid's forecasts, the transition between available and desired forecast resolution is not as straightforward since the change is into the direction of finer resolution. To overcome this problem, a synthetic time series is created for onshore wind and consumption forecasts with the help of minute level measurement data [71]. The creation principle of these synthetic time series is illustrated in Figure 10 below.

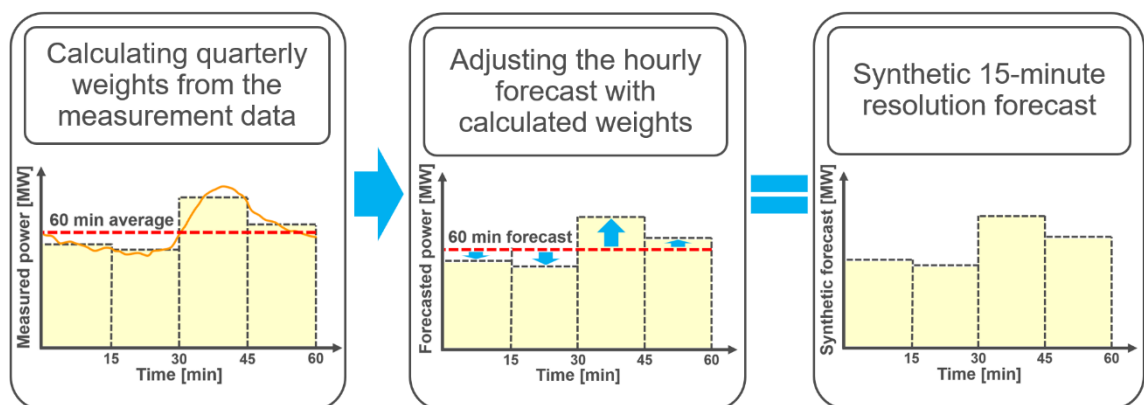


Figure 10: Overview of the synthetic 15-minute resolution forecast creation process. The x-axis illustrates minutes from the beginning of the hour.

The creation of synthetic forecasts starts by calculating weights from the historical measurement data. In practice these weights correspond to percentages of the hourly averages, and they are calculated by dividing the difference between the 15-minute and 60-

minute averages with the hourly average and adding one to the created division. After this initial step, the hourly resolution forecast data is scaled with the obtained weights on a quarter-hourly level. As a result of this weighting process, a synthetic 15-minute resolution forecast is created.

The advantage of this approach is its ability to maintain the predicted energy content at the hourly level while following the trend of actualized production or consumption. It can also capture large intra-hour deviations while keeping the implementation simple. However, it is good to note that the ability to follow the actualized power may lead to over optimistic forecast accuracy, as the synthetic forecast always corrects the quarterly values into right direction compared to 60-minute forecast. Thus, the real 15-minute forecast errors may be much larger if the forecast predicts the trend of actual power incorrectly.

In addition to the three main processing needs, some fine tuning is required before continuing to the forecast error calculation phase. Firstly, all times with zero predicted production according to the day-ahead forecast are excluded from the collected PV datasets. This is simply done to reduce the amount of data processed in the later steps, as the zero values do not give any additional information about the behavior of forecast errors. Secondly, the datapoints related to the electricity trading error in 24th of November 2023, are removed from the consumption datasets [91]. Finally, the gathered ACE OL time series is modified by removing all quarter-hours with 10 second average frequency values outside the range of 49.85 – 50.15 Hz. The choice of this range is based on frequency quality analysis of the previous year's [92].

4.2.2 Clustering the forecast error data

After finishing the described preprocessing stage, quarterly per unit forecast errors are calculated for the wind, PV, and consumption forecasts by using Equations 6 and 7. This calculation is performed separately for the day-ahead and 1-hour prediction horizon forecasts. Next, the obtained datasets are clustered with *k-means++* algorithm [93]. The chosen clustering technique is a variant of the *k-means* method, which is a widely used clustering technique with a simple implementation and fast runtime. On a general level, clustering is a data analysis process in which a set of objects is divided into groups (clusters) in a way that objects similar to each other end up in the same group [94]. The similarity of these objects is defined by their features [95].

In the case of day-ahead onshore and offshore wind power forecast errors, the clustering is performed according to three features: measured quarter-hourly average production,

change in the measured production between consecutive hours and used forecast horizon. The first two features are scaled with the related installed capacity and the third feature is scaled with the length of the longest prediction horizon, in order to have the features in a common range [95]. While clustering the forecast error data with 1-hour prediction horizon, the third feature is left out. The decision to use measured power relates to the dependency of production level and predictability explained earlier in section 2.3. The change between hours, on the other hand, is chosen based on an idea that high changes correlate with times of significant weather fronts. Finally, the third feature can be justified by the known dependency of forecast horizon and accuracy.

Clustering of the PV forecast error data differs from the wind power clustering by using scaled average GHlc of the related quarter-hour (scaled with the maximum annual average quarter-hourly GHlc of the related location), instead of the measured production. The first reason for this choice is the PV production's dependency on deterministic factors such as time of the day and season [65]. For example, identical production levels could occur during cloudy summer days and clear autumn days, but the uncertainties of the related forecasts would be entirely different.

The second reason to use irradiation data relates to its dependency on the geographical location. In practice, using the scaled GHlc enables matching the Danish PV forecast error data with the irradiation values available in Finland. The decision to use the production changes as a feature is reasoned by an idea that large hourly differences correlate with times of significant changes in the overall cloudiness and are thus more vulnerable to forecast errors. It is also important to note, that since the one-hour prediction horizon PV forecast has false zero values due to its limited updating cycle, only data-points with positive forecasted power are used while clustering the 1-hour prediction horizon error data [73].

The features used in the clustering of consumption forecast error data are near identical to ones used with wind production, but now the feature scaling is done according to the hourly average peak demand of the corresponding year. Also the reasoning differs slightly from the wind power, as the changes between consecutive hours are thought to describe the uncertainty related to the daily consumption ramping periods, such as the morning ramp around hours 6 am to 9 am in Finnish local time [92]. The level of consumption as a feature can be justified simply by the magnitude of possible forecast errors with different power levels.

Since the k-means and k-means++ differ from each other only by their initializing method, the k-means algorithm is presented first to have a basic understanding of the working

principle of the chosen method [93]. The k-means algorithm aims to define k cluster centers that minimize the cost function defined by Equation 8:

$$cost(P, C) := \sum_{p \in P} \min_{c \in C} \|p - c\|^2, \quad (8)$$

where $P \subset \mathbb{R}^d$ denotes a set of datapoints p and $C \subset \mathbb{R}^d$ is a set of cluster centers c [94]. The notation \mathbb{R}^d refers to Euclidean space of dimension d in which the datapoints and cluster centers are located. By searching for an optimal solution for the defined cost function, the k-means algorithm tries to minimize the sum of squared distances between each datapoint and its closest cluster center [93].

The k-means algorithm starts by arbitrarily choosing k initial cluster centers [94]. After the initializing phase, the algorithm defines k clusters by assigning each datapoint in P to cluster which center is nearest to the datapoint in question. Next, the algorithm calculates the center of mass for each cluster from the assigned datapoints and updates the related cluster center to this calculated value. After this, steps following the initializing phase are repeated until C is no longer changing. As the datapoints are assigned to the nearest center during each iteration, the k-means algorithm implicitly partitions the data to clusters G_m , in which $m = \{1, \dots, k\}$.

The idea of k-means++ is to increase the accuracy of the k-means method and reduce the running time of the algorithm [93]. The initialization phase of the augmented method starts by choosing one cluster center uniformly at random from the dataset P . After this, rest of the cluster centers are chosen randomly from the same dataset but now the datapoints are given probabilities before the selection. This probability is high if the datapoint is far away from already chosen cluster centers and low if vice versa. The second step of the initialization algorithm is repeated until k cluster centers are defined. After this, k-means++ follows the steps of the already explained k-means algorithm.

4.2.3 Defining the number of clusters for k-means++ -algorithm

Increasing the number of clusters naturally reduces the value of the defined cost function [94]. On the other hand, a higher number of clusters results in less data in one cluster, which increases the significance of a single datapoint while forming the conditional error PDFs [65]. This will in turn make the analysis more prone to extreme errors, as only few observations may increase the reserve requirements considerably. To overcome this optimization problem, a parallel calculation process to the actual balancing need study is performed. The word parallel is used now to highlight the fact that this calculation is

performed as a separate process from the one summarized in Figure 9, as it requires a complete calculation model.

On a high level, the number of clusters is optimized by creating multiple calculation models and testing them against Finnish ACE OL time series from the year 2023 [65]. The tested models differ from each other by using different sets of conditional PDFs while forming the joint distributions. These PDF sets diverge in turn by the number of clusters used while dividing the forecast error data into subgroups, and thus by comparing the performance of the created models, the number of clusters can be optimized. The model performance is evaluated in this work by comparing the realized quarter-hourly average ACE OL values to the joint PDFs proposed by the related calculation model. In this comparison, the ACE OL values are combined with the right PDFs by first adding the needed features to the ACE OL dataset and then running the calculation model as if the ACE OL dataset was a market simulation result time series.

In a more technical level, the described comparison is based on Continuous Ranked Probability Score (CRPS) calculation, which is defined for a single quarter-hour by Equations 9 and 10 [96][97]:

$$CRPS(F, z) = \int_{-\infty}^{\infty} \left(F_{joint\ PDF}(x) - \mathbb{1}(x \geq z) \right)^2 dx \quad (9)$$

$$\mathbb{1}(x \geq z) = \begin{cases} 0, & x < z \\ 1, & x \geq z \end{cases} \quad (10)$$

In the equations above $F_{joint\ PDF}(x)$ is the Cumulative Distribution Function (CDF) of the joint PDF, x refers to a point at the CDF's x-axis in MW and z denotes the realized ACE OL value in MW [96][97]. The CRPS is calculated for every quarter-hour of the year and the related calculation model is scored according to the mean of these scores [96]. To further clarify the CRPS calculation, Figure 11 highlights the relation between the integrand of Equation 9, CDF of the joint PDF and CDF of the realized ACE OL.

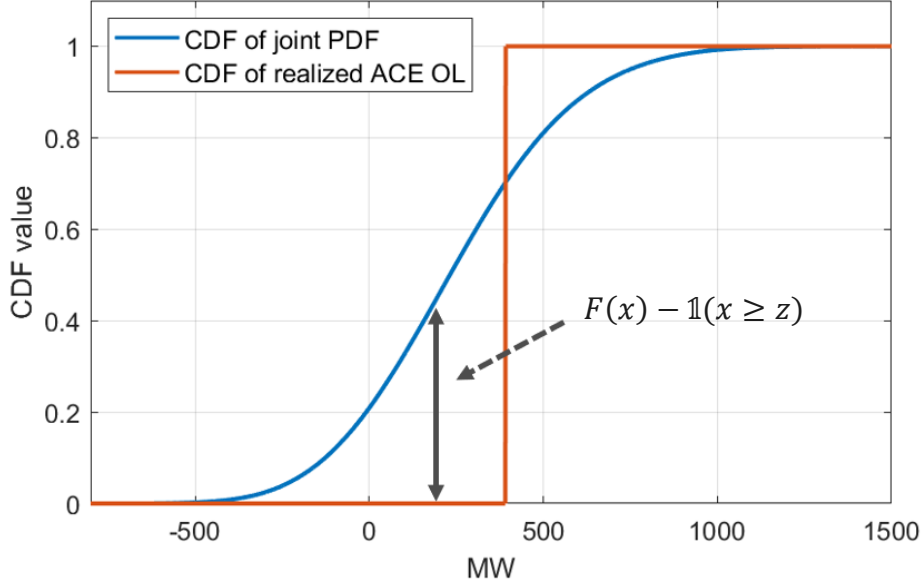


Figure 11: Demonstration of the CRPS calculation for a single quarter-hour of the year 2023. In the case of ideal balancing need calculation model, the area between the CDF curves would be zero for every quarter-hour.

To limit the calculation workload, the optimal solution is searched from the range of 80 to 180 clusters and the step size of this iteration is set to 20 clusters. The lower limit of this range is reasoned by the results of [65] which ended up to 40 clusters, while clustering one year of quarter-hourly data according to a single feature. The upper limit is in turn set heuristically to avoid the sensitivity problem described in the first paragraph of this sub-section. Also, since the model's behavior is highly dependent on the division between day-ahead and 1-hour prediction horizon forecasts and the improvement percentages, conservative sub-scenario described earlier in Figure 8 is chosen for the CRPS calculation. As a result of this iteration, the number of 120 clusters is considered the optimal choice for the calculation model applied in the latter case study. With 120 clusters, the model reached CRPS score of 206.522.

4.2.4 Creation of the conditional PDFs

In the last step of phase one, conditional PDFs are estimated for each cluster formed by the k-means++ algorithm. These PDFs are created by using kernel density estimation, which enables PDF fitting without making assumptions about the distribution of the underlying data [98]. The kernel density estimator is calculated with Equation 11 for the forecast type i and cluster m :

$$f_m(u) = \frac{1}{Nh_m} \sum_{t \in G_m} K\left(\frac{u - \epsilon_{i,t}^{pu}}{h_m}\right), \quad (11)$$

where $f_m(u)$ is the kernel estimator in evaluation point u , N denotes the number of samples in cluster m , h_m is the bandwidth of the kernel estimator and $K(\cdot)$ refers to the kernel smoothing function [99]. The kernel smoothing function is defined in this work as a normal probability density function, based on the previous studies using similar approach [65][66][74].

The bandwidth h_m is in turn defined with Silverman's rule of thumb, which gives an ideal bandwidth in case of Gaussian smoothing function and normally distributed data [99]. Although the premises of this method are not entirely met, using a simple rule of thumb is considered justified, as the more complex approaches such as cross-validation [100] would increase the computational work substantially. The Silverman's rule is defined with Equation 12 below:

$$h_m = \left(\frac{4}{3N} \right)^{0.2} \sigma_m, \quad (12)$$

where σ_m is the standard deviation of the data in cluster m [99]. To make this approach more suitable for long-tailed distributions and diminish the effect of outliers, it can be enhanced by using the median absolute estimator $\hat{\sigma}_m$ instead of standard deviation [101]. This estimator is calculated with Equation 13 [101]:

$$\hat{\sigma}_m = \frac{\text{median}|\epsilon_{i,t}^{pu} - \text{median}(\epsilon_{i,t}^{pu})|}{0.6745}, t \in G_m. \quad (13)$$

After creating the PDFs for every cluster, the formed distributions are saved into the database. This will reduce the calculation workload if the balancing need analysis is performed later with different market simulation results or assumptions considering the market behavior or forecast accuracy.

4.3 Phase 2: Market simulations

On a general level, the used market model tries to minimize the system cost for one year, while respecting constraints defined in the model initialization [53]. These constraints include for example available transmission infrastructure, fuel prices and production capacities. Besides price and capacity constraints, the model utilizes hourly weather time series to estimate production and consumption values in future scenarios. These weather time series include variables such as rainfall, wind speed and temperature, and are based on some specified historical climate year. In this work the constraints are derived from the base cases introduced in sub-section 3.5 and the used weather time series correspond to climate years defined in the same sub-section.

After initializing the model according to the examined cases, simulations for 8760 hours are performed separately for every base case and iterated according to different climate years. As a result of these simulations, a total of 12 hourly time series of production and consumption are created. During the simulations, production and transmission capacities are kept constant throughout the modeled year [53]. It is also important to note that some of the wind and PV production operates below maximum power point, if the electricity price proposed by the market model goes below a certain threshold.

To use the market simulation results later in the actual balancing need calculation, they must be augmented with features. In practice, the features related to pu production or consumption, pu changes between consecutive hours and forecast horizon are derived straight from the production and consumption time series created during the market simulations. The scaling of power related features is performed by using installed capacities of the examined cases or the maximum hourly demand appearing in the simulated consumption time series. The needed pu irradiation dataset is in turn computed from the irradiation data of Jyväskylä by scaling the 15-minute average values with the maximum annual quarter-hourly irradiation of Aarhus. By applying the Danish maximum value for scaling, the created pu irradiation time series will align the error PDFs properly with the Finnish irradiation conditions.

4.4 Phase 3: Calculating the balancing needs

In the final phase of the thesis approach, balancing needs are estimated for each base case by using three different sub-scenarios and climate years. As this calculation process is nearly identical between the examined cases, the following paragraphs describe its implementation for a single sub-scenario with one climate year. The explanation is also performed on an hourly level, as the calculation's internal steps are performed separately for every hour of the examined year.

During the first step of this hourly calculation process, a set of conditional forecast error distributions are defined for the hour in question, based on their proximity to the conditions described by the market simulations. In a more technical level, this PDF selection is done by using k-Nearest Neighbours (k-NN) classifier [102]. The basic idea of k-NN is to classify new datapoints based on the classes of their nearest neighbours.

In this work these classes correspond to the clusters used while creating the conditional error PDFs. The number of nearest neighbours is restricted to one, since there are no visible class boundaries inside the Euclidean space, in which the pu forecast error data-

points are positioned during the clustering. Finally, the nearness is defined as the Euclidean distance of pu forecast error datapoints and the market simulation results positioned in the same Euclidean space, based on their attached features. It is also worth highlighting that the forecast type specific PDFs are defined individually, as different forecast types have their own Euclidean spaces and unique features.

4.4.1 Forming a joint PDF for the modeled uncertainty factors

Next, the selected per unit PDFs are scaled back to MW values as described in the beginning of sub-section 4.2. However, now the upscaling is adjusted pursuant to the scenario specific market behavior and forecast accuracy assumptions. Also, the targeted calculation accuracy is considered while defining the number of samples.

For example, while calculating the balancing needs with the **moderate sub-scenario**, the sample numbers used in the upscaling of **consumption** PDFs are multiplied by 0.25 in the case of day-ahead error PDFs and by 0.75 in the case of 1-hour error distributions. After performing the market behavior and accuracy related adjustments, the defined sample numbers are scaled by 50 to change the sampling resolution from 1 MW to 20 kW. The sampling resolution refers now to the distance between two adjacent samples in the x-axis of sampled PDF. Using higher resolution will mitigate the distortion created by the next calculation step and thus increase the overall accuracy of the used approach.

After finding the most representative error distributions and scaling them back to MW values, the gathered PDFs are combined with convolution. Convolution is defined in the case of two random variables X and Y and their sum $Z = X + Y$ with Equations 14 and 15 below [66]:

$$f_Z = f_X * f_Y \quad (14)$$

$$f_Z(x) = \sum_{n=-\infty}^{\infty} f_X(n) \cdot f_Y(x - n). \quad (15)$$

In the upper equation, f_Z denotes the joint PDF of the resulting random variable Z , f_X and f_Y are the PDFs of random variables X and Y , and the asterisk is used to mark the convolution operation [66]. In the second equation, $f_Z(x)$ denotes the probability density at point x in the x-axis of convolved PDF and variable n is used sweep through the x-axes of input PDFs f_X and f_Y .

As the thesis approach is based on estimating forecast error PDFs with day-ahead and 1-hour prediction horizons for 4 different uncertainty sources, the operation defined with

Equation 15 is repeated until a total of 8 different PDFs are joined together. This operation is presented below with Equation 16:

$$f_{joint\ PDF} = f_{PV,DA} * f_{PV,1h} * f_{offshore\ wind,DA} * f_{offshore\ wind,1h} * f_{wind,DA} * f_{wind,1h} * f_{consumption,DA} * f_{consumption,1h} , \quad (16)$$

where the first subscripts define the forecast types and the second subscripts specify the forecast horizons used while estimating the error distributions [66]. Onshore wind is now denoted simply as *wind* to avoid splitting the equation into three rows. By evaluating Equation 16, a joint PDF for the modeled uncertainty factors is created.

4.4.2 Applying reliability level for the joint PDF

In the last step of the hourly calculation process, balancing needs are estimated from the joint PDF by using predefined reliability level. The results of this calculation can be interpreted as the amount of combined mFRR and aFRR capacity, which is adequate to compensate imbalances arising from the modeled uncertainty factors for 97 % of the time, in system conditions described by the market model. Since the used reliability level ρ_{RL} considers both up and down directions, surplus $\rho_{surplus}$ and deficit $\rho_{deficit}$ probabilities are defined for the actual balancing need calculation [72]. These probabilities describe the fraction of time during which a shortage of downward or upward reserves is accepted, and they are calculated with Equation 17 [66][72]:

$$\rho_{surplus} = \rho_{deficit} = \frac{100\% - \rho_{RL}}{2} . \quad (17)$$

After defining the surplus and deficit probabilities, the upward and downward balancing needs are derived by searching CDF values for the joint PDF that are fulfilling the conditions defined by Equations 18 and 19 [66]:

$$F_{joint\ PDF}(R_{down}) \geq 1 - \rho_{surplus} \quad (18)$$

$$F_{joint\ PDF}(R_{up}) \leq \rho_{deficit} . \quad (19)$$

In the equations above, R_{down} refers to the downward balancing needs and R_{up} to the upward balancing needs. The CDF of the joint uncertainty PDF is in turn defined with Equation 20 below [66]:

$$F_{joint\ PDF}(x) = \int_{-\infty}^x f_{joint\ PDF}(x) dx . \quad (20)$$

To provide more insight to the relation between the uncertainty PDF, reliability level and balancing needs, Figure 12 is illustrating a joint distribution created by using the moderate sub-scenario and market simulation results from the year 2026. The vertical dashed

lines drawn in the figure present the defined balancing needs in up and down direction. Consequently, the area enclosed by these lines is equal to the defined reliability level.

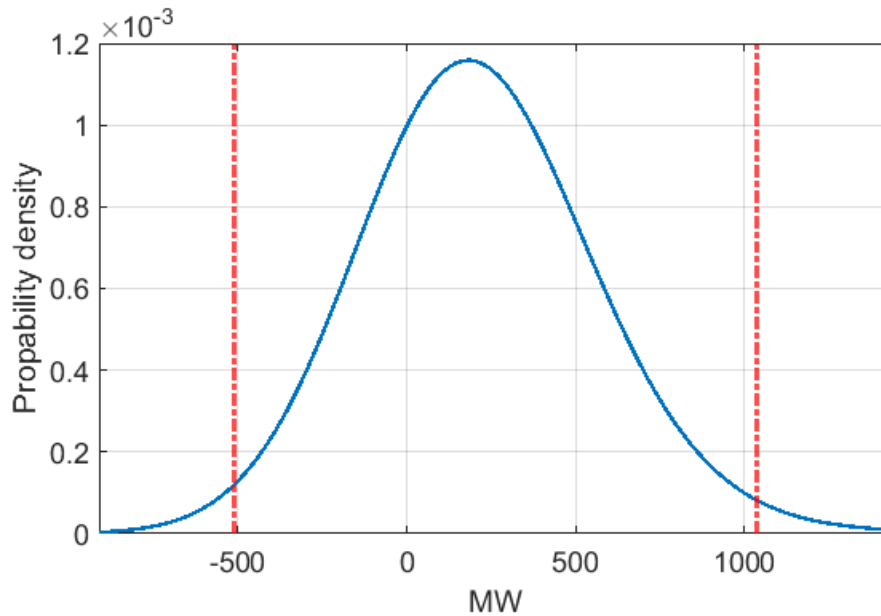


Figure 12: Joint uncertainty PDF in moderate sub-scenario during the year 2026 and mid-wind climate year. The dashed vertical lines are marking the defined hourly balancing needs. During the hour in question, per unit wind production was 0.94827, consumption was 0.78231 and irradiation was zero.

As the calculation steps presented earlier in this sub-section are defined for a single hour, they are naturally repeated until a time series of 8760 hours is created for every examined scenario. The reason to perform this calculation on hourly resolution, although the used error PDFs are created with quarter-hourly data, is simply due to the limited resolution of the market simulations [53]. This limitation is also the reason to apply the change in per unit power between consecutive hours instead of quarters, while clustering the forecast error data.

5. CASE STUDY

In this section, a case study is performed by applying the methodology described in the previous chapter. The main objective of this study is to estimate quarter-hourly balancing needs in the scenarios defined earlier in sub-section 3.5. As a recap, balancing needs are estimated in four base cases corresponding to projected development of the years 2026, 2028, 2030 and 2033. Within each base case, assumptions related to BRPs' market behavior and forecast accuracy are varied, leading to conservative, moderate and advanced sub-scenarios. To further increase the robustness of the analysis, these sub-scenarios are calculated by using three different climate year's corresponding to low, mid, and high annual wind conditions.

Although the essence of this chapter is to analyze the results of the performed case study, it starts by benchmarking the created calculation model. During this validation phase, the created model is tested against historical ACE OL time series from the first half of the year 2024. Also, hourly ramping of wind power, PV and consumption is analyzed in the end of this chapter by using the market simulation data generated originally for the case study.

5.1 Testing the created calculation model

The model validation can be divided into three phases. It starts by computing the proportion of quarter-hours during which the estimated reserve capacity is sufficient to cover the realized ACE OL values. Besides to this empirical reliability level, the minimum difference between proposed up- or downwards reserve and related ACE OL value is calculated during the first validation phase for every quarter-hour with adequate capacity. These margins will give valuable information on how probable the model is to overestimate the future balancing needs. In this sub-section, the term reserve capacity matches the definition of estimated balancing needs but is preferred, as it describes the test setting more accurately. The calculation of empirical reliability level and margins is performed by using reliability level of 97 % and conservative sub-scenario. The results of this calculation are summarized in Table 1 below.

Table 1: Empirical reliability level and key figures derived from the calculated margins. The ACE OL data used for this calculation was gathered from the first two quartiles of the year 2024 and reliability level of 97 % was applied.

Empirical reliability level (%)	Margins (MW)		
	10 th percentile	Average	90 th percentile
90.82	153	576	1001

The calculation of the empirical reliability level presented in this sub-section was also used to select the 97 % reliability level declared earlier in the work. In practice, this decision was done by performing the computation explained in the first paragraph with several different reliability levels and choosing the smallest reliability level which exceeded an empirical level of 90 % for the first time. This iteration started from 95 % reliability level and proceeded with one percentage steps. The threshold of 90 % is reasoned by an idea that since the model considers only forecast errors, it is unlikely to reach the applied reliability level even in the case of ideal forecast error model. The second reason for limiting the targeted empirical reliability level to 90 % is the model's sensitiveness towards outliers in the historical forecast error data when using higher reliability levels.

In the second part of the validation process, CRPS value for the ACE OL data of the year 2024 is computed. This calculation is performed by using the method explained earlier in sub-section 4.2.3. When applying conservative sub-scenario, the model reaches CRPS of 266.994. The probable reason why this value differs substantially from the one computed for the year 2023 (206.522), relates to the up scaling of pu error distributions. In practice, the PDFs become wider as the installed production capacity or peak demand used for the scaling increases. This will in turn lead to increased CRPS values without necessarily losing the performance of the calculation model. For this reason, the obtained CRPS cannot be directly compared to one from the year 2023. However, this value can be used later as a benchmark if the created model is developed further.

The third phase of the validation process focuses on those moments during which the capacity proposed by the model is insufficient to cover the realized ACE OL values. Similarly to the first part, minimum differences between estimated reserve capacities and ACE OL values are computed. However, now this calculation considers only quarter-hours with inadequate capacity. Some key figures derived from this exceedance time series are presented in Table 2 below. The first column of the table is used to highlight whether the exceedance of proposed reserve capacity occurred during up- or downward balancing needs.

Table 2: Key figures derived from the calculated exceedance time series. The ACE OL data used for this calculation was gathered from the first two quartiles of the year 2024 and reliability level of 97 % was applied.

Direction	Reserve capacity exceedances (MW)		
	10 th percentile	Average	90 th percentile
Upward	25	165	409
Downward	17	169	361

To further characterize the drawbacks of the calculation model, Figure 13 illustrates the quarter-hours during which the proposed capacity was inadequate to cover realized ACE OL values as a function of per unit consumption, onshore wind power and irradiation.

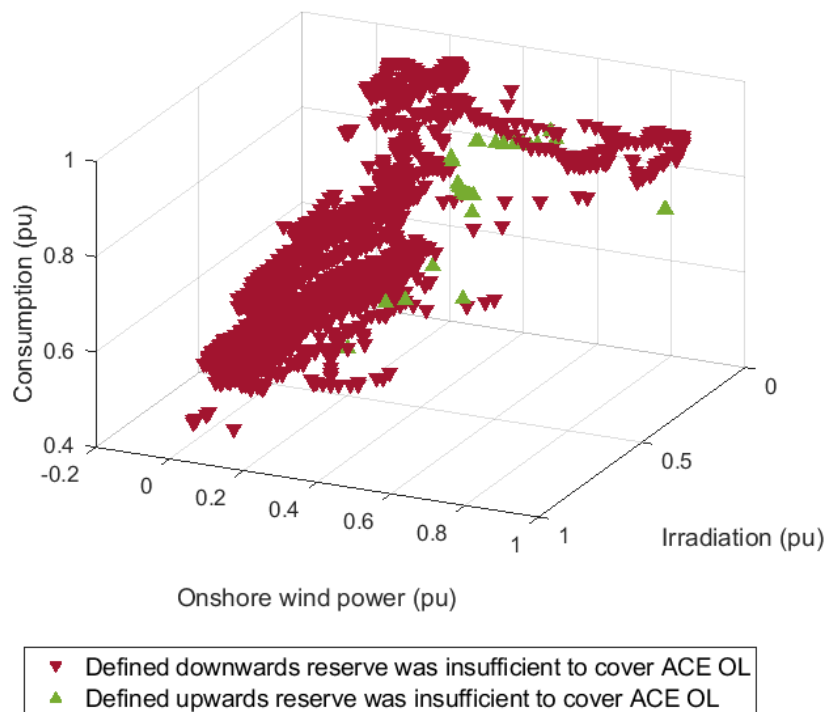


Figure 13: Quarter-hours during which the calculation model was unable to propose enough reserve capacity to cover realized ACE OL values. The quarter-hours are plotted as a function of their related system conditions. The ACE OL data used for this calculation was gathered from the first two quartiles of the year 2024 and reliability level of 97 % was applied.

Based on Figure 13, it seems that the calculation model is more likely to propose insufficient downward reserve capacity than upward capacity. However, this observation should be taken with some caution, since about 75 % of the ACE OL data used in testing consisted of positive values, which are in turn related to the downward balancing needs. Besides the directional variation in the performance, calm weather with low demand appears to be a challenging condition for the calculation model to estimate the reserve needs sufficiently.

While analyzing the missed quarters in terms of production and consumption changes between consecutive hours, most of these instances were linked to positive upward changes in PV and consumption. The length of the forecast horizon, on the other hand, does not appear to have tendency for higher or lower model failure rate. Before proceeding to the actual case study, it is important to highlight that as the model considers only forecast errors, analysis performed especially in the last phase of the validation process, should be considered as directional.

5.2 Balancing needs in the examined cases

To visualize the results of the performed case study, duration curves are drawn for the estimated balancing needs. The aim of these graphs is to give general understanding on how large the balancing needs are and how much they vary within the examined scenarios. These curves will also provide insight on how forecast accuracy development and BRPs' market behavior affects the balancing needs, as different sub-scenarios are presented for each year. The resulting Figure 14, including all formed duration curves for the mid-wind climate year, is shown below.

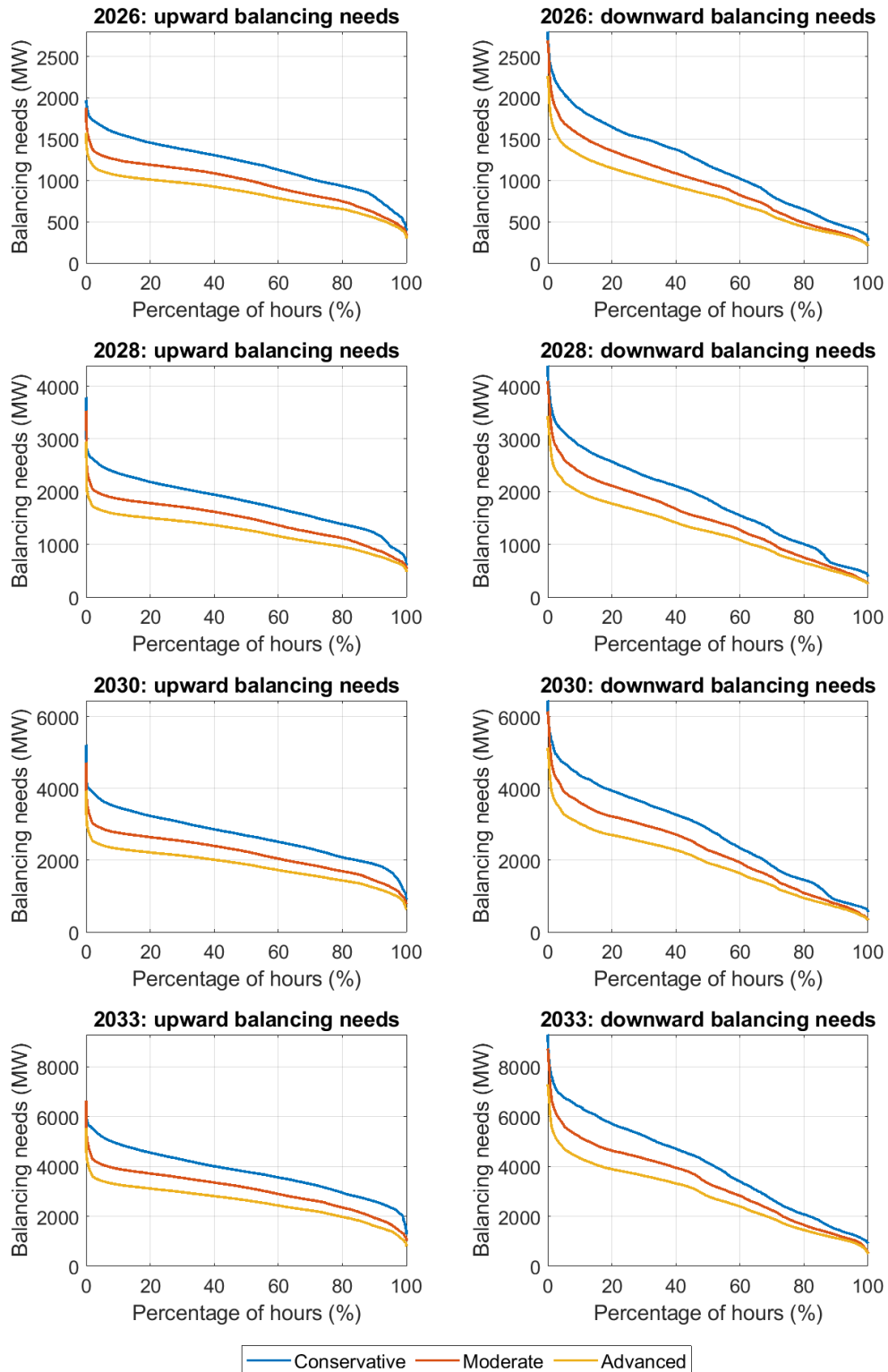


Figure 14: Duration curves of the estimated balancing needs within different years (base cases) and sub-scenarios. The market simulation data used for the calculation of the presented balancing needs was created by applying mid-wind climate year.

By studying the behavior of duration curves within different sub-scenarios, it becomes clear that assumptions considering market behavior and forecast accuracy have a major

impact on the development of balancing needs. For example, when comparing the upward balancing needs in 2033 between conservative and advanced sub-scenarios, there is a difference of close to 1500 MW around 20 % mark. Another important observation to be made from the presented figure is that the effect of applied sub-scenario remains more consistent throughout the percentages with upward balancing needs, than in the case of opposite direction.

To highlight the seasonal variation of balancing needs, and their dependency on production and consumption level, Figures 15 and 16 are drawn for the first and last examined year. This hourly review is performed by using mid-wind climate year and moderate sub-scenario. The production, consumption and balancing need time series presented in the next figures are 72 hour moving averages of the original time series, since using unfiltered data would make the figures unclear. Similar figures created for the years 2028 and 2030 can be found from Appendix A of this thesis.

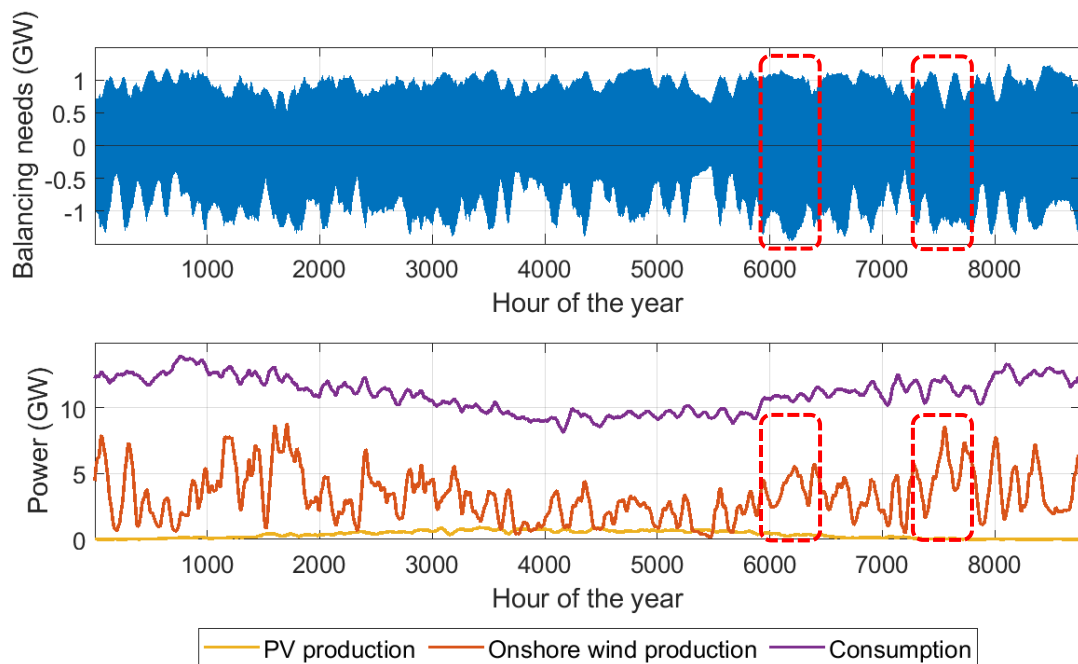


Figure 15: The upper graph presents hourly balancing needs for the year 2026 while applying moderate sub-scenario and mid-wind climate year. Positive values indicate upward balancing needs and negative values correspond to downward balancing needs. The lower graph illustrates production and consumption values of the same scenario. Since plotting the unfiltered time series would make the figure hard to interpret, 72 hour moving averages of the related time series are used instead.

As depicted in the preceding figure, the balancing needs are highly dependent on the wind power production level. This dependency seems to be particularly strong with downward balancing needs, explaining the previously observed difference in the behavior of upward and downward balancing need duration curves. In practice, the choice of applied

sub-scenario has the greatest impact on the error distributions of wind and PV production, and thus it is natural that the duration curves diverge in the case of downward balancing needs, when the above-mentioned relation exists.

However, this connection is far from linear, which becomes clear when comparing the periods highlighted with dashed rectangles. During the first highlighted period, the estimated balancing needs are close to the annual maximum values, although wind power production is near mid-range levels. Within the second period, wind power production is close to its installed capacity, but now both up and down balancing needs are significantly reduced compared to the first period. This behavior is likely due to the cubic relationship between wind speed and generated power and the stabilization of production, discussed earlier in sub-section 2.3.1.

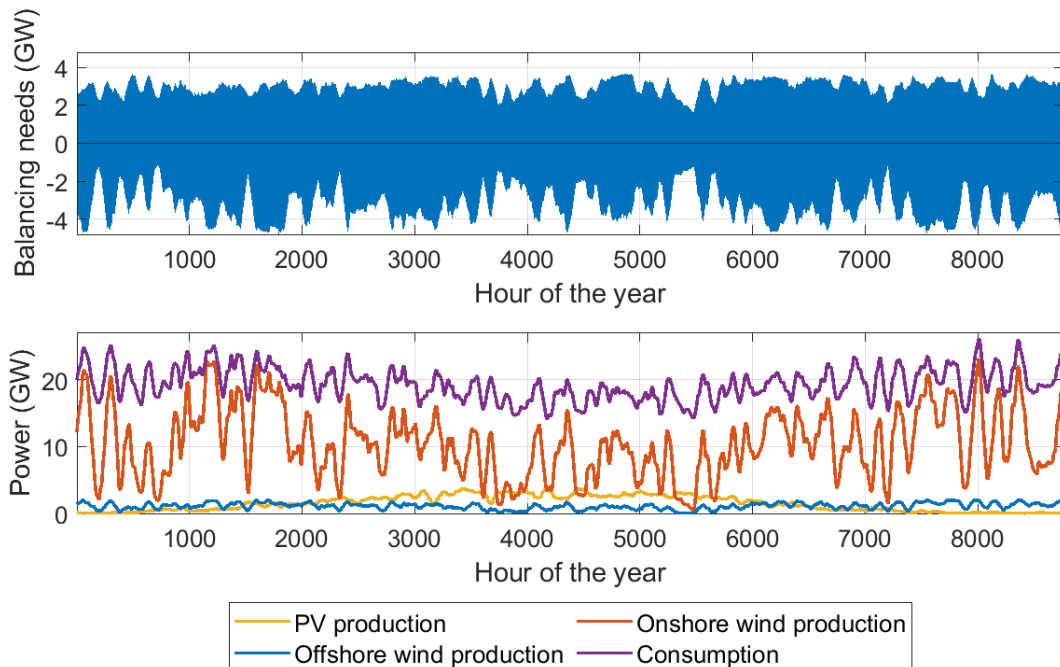


Figure 16: The upper graph presents hourly balancing needs for the year 2033 while applying moderate sub-scenario and mid-wind climate year. Positive values indicate upward balancing needs and negative values correspond to downward balancing needs. The lower graph illustrates production and consumption values of the same scenario. Since plotting the unfiltered time series would make the figure hard to interpret, 72 hour moving averages of the related time series are used instead.

Similar observations about the dependency between wind power and balancing needs can be made also from the results of the year 2033. Although, this time the reduction of balancing needs during the peak production periods is not as evident as in the year 2026. The first probable explanation for the deterioration of this phenomena is that the highest wind power production values are far from the installed capacity, due to increased geographical aggregation and curtailment created by the negative day-ahead prices [53]. Secondly, as the consumption follows the available production more dynamically during

the year 2033 than in 2026, it is likely that the increased uncertainty of consumption outweighs the possible reduction of balancing needs created by the stabilization of wind power production. However, it should be noted that since the used calculation model selects the PDFs partly based on the pu production level, it may use incorrect PDFs to model the remaining part of production which is still operating during the curtailment periods. In other words, there could be still some hours in the year 2033 during which the balancing needs would decrease due to the saturation of wind production.

Next, key figures computed from the results of different sub-scenarios and climate years are presented in Tables 3 and 4 below. The aim of these charts is to show how the climate years affect the balancing needs and simplify the comparison between the examined years and different sub-scenarios.

Table 3: Minimum, average, and maximum upward balancing needs within different sub-scenarios and climate years. The numerical values under the sub-scenario column are expressed in MW.

Base case	Climate year	Sub-scenarios								
		Conservative			Moderate			Advanced		
		Min	Avg	Max	Min	Avg	Max	Min	Avg	Max
2026	Low wind	393	1180	2133	307	949	1871	245	816	1569
	Mid wind	395	1196	1968	328	968	1876	295	833	1580
	High wind	400	1182	2162	333	960	2012	300	825	1683
2028	Low wind	537	1777	3464	469	1435	3465	411	1219	2898
	Mid wind	608	1789	3782	530	1449	3528	473	1231	2947
	High wind	558	1785	3600	492	1450	3526	432	1233	2949
2030	Low wind	1049	2631	4872	807	2114	4939	641	1782	4139
	Mid wind	904	2675	5211	791	2173	4714	634	1831	3939
	High wind	938	2710	5172	806	2208	5169	640	1862	4313
2033	Low wind	1509	3654	6830	996	2893	6888	790	2417	5756
	Mid wind	1268	3769	6594	1005	3041	6627	795	2548	5535
	High wind	1288	3877	7637	1068	3139	7233	847	2634	6036

Table 4: Minimum, average, and maximum downward balancing needs within different sub-scenarios and climate years. The numerical values under the sub-scenario column are expressed in MW.

Base case	Climate year	Sub-scenarios								
		Conservative			Moderate			Advanced		
		Min	Avg	Max	Min	Avg	Max	Min	Avg	Max
2026	Low wind	198	1080	2861	174	882	2702	158	761	2268
	Mid wind	269	1186	2800	203	966	2693	201	828	2264
	High wind	312	1281	2857	218	1048	2692	215	897	2253
2028	Low wind	284	1722	4341	212	1405	4078	205	1194	3409
	Mid wind	387	1814	4386	256	1481	4099	251	1256	3431
	High wind	383	1960	4338	255	1608	4107	253	1361	3437
2030	Low wind	527	2456	6478	304	2024	6069	288	1713	5059
	Mid wind	555	2758	6448	345	2269	6141	327	1916	5130
	High wind	564	2980	6474	327	2455	6125	314	2067	5115
2033	Low wind	867	3612	9212	471	3009	8709	448	2561	7266
	Mid wind	903	4006	9276	527	3307	8707	500	2797	7277
	High wind	871	4318	9251	520	3559	8755	494	2999	7303

When comparing the averages of Tables 3 and 4 within different sub-scenarios, it can be noted that the effect of climate years is most significant with the downward balancing needs. This observation is in line with the previously discussed relationship between wind production and balancing needs, and the choice of climate years based on their annual wind conditions. However, if a similar comparison is performed for the maximum values, the differences become almost negligible with the downward needs. One possible explanation for this behavior is that there are some hours within all climate years, which are challenging enough to trigger the usage of most right tailed PDFs in the calculation. With upward balancing needs, there is no similar saturation effect visible.

The differences between average balancing needs of the examined sub-scenarios are in turn quite similar for both directions, when the comparison is done one base case and climate year at a time. The likely reason for this, somewhat surprising finding, is the upscaling of pu PDFs during the calculation. In practice, as the internal characteristics of the different sub-scenarios are considered through scaling of pu PDFs, the differences between their results originate also from this scaling process and are thus quite similar in both directions.

When analyzing the yearly development within different sub-scenarios, the growth of balancing needs stays relative stable and follows the trend of consumption and renewable production, illustrated previously in Figure 7. This is an expected result, since the differences in the installed capacities and consumption levels are also modeled through the scaling of pu PDFs. However, it is good to note that some sub-scenarios are more descriptive during certain years than others. For example, if we assume that the conservative sub-scenario best describes the year 2026, moderate the years 2028-2030 and advanced the year 2033, the development of the balancing needs begins to resemble an s-curve instead of a linear or cubic growth.

5.3 Ramping of production and consumption in the examined cases

This section analyses the ramping of wind power, PV and consumption by using the market simulation data created originally for the case study. Also, development of deterministic imbalances created by the different ramping speeds is discussed briefly. The main reason to limit the analysis of ramping to the above listed production sources, is their anticipated growth within the scope of this thesis.

Since the market simulation data is limited to hourly resolution, the ramping values presented in this section must be interpreted as highly directional. In practice, the quarterly ramping values can range anywhere from 0 % up to 100 % or even higher portions of the hourly ramping values, depending on the sub-hourly behavior of production or consumption and the quarter-hour in question. Another point to consider while examining the computed ramping values, is that their descriptiveness depends also on how actively the market actors utilize the quarter-hourly trading. For example, if one assumes that the market participants trade mainly with hourly resolution, the presented values can be considered to describe the actual ramping values relatively well, and vice versa if the finer market resolution is applied widely.

Figures 17 and 18 present the first and last 20 % of the hourly ramping duration curves computed for the years 2026, 2028, 2030 and 2033. The duration curves are drawn by using market simulation data created with mid-wind climate year. Since the market model considers the possible curtailment of wind and PV production during the negative day-ahead prices, the price-induced ramping is included in the presented values. To make the graphs easier to interpret, y-axes of the figures are limited to include 99.5 % of the largest ramping values in the direction in question. These graphs include also reference duration curves to provide context for the observed values, and they are computed from the historical measurement data of the year 2023.

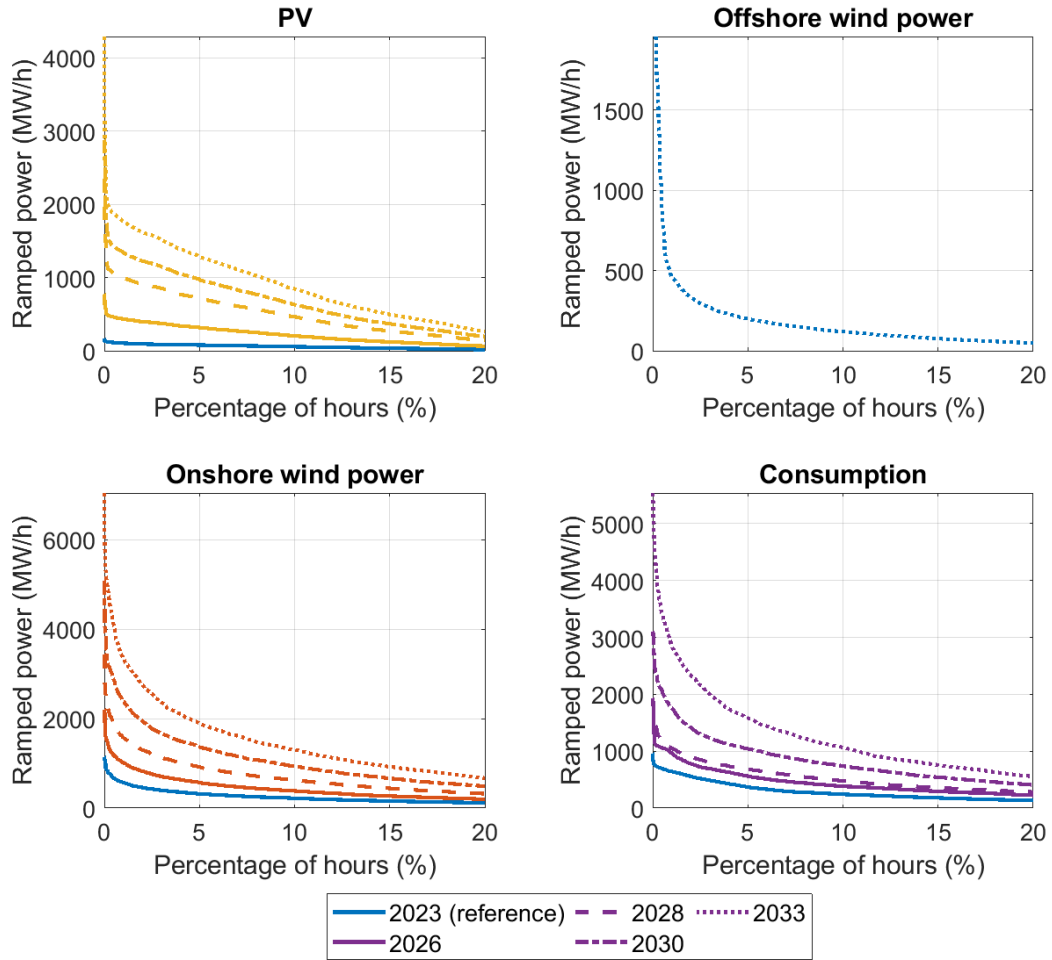


Figure 17: The first 20 % of the hourly ramping duration curves. Market simulation data used in this figure was created by applying mid-wind climate year. The reference duration curve is calculated from the historical measurement data of the year 2023. To distinguish the lines from each other, top 0.5 % upward ramping values from the year 2033 are excluded from the figures.

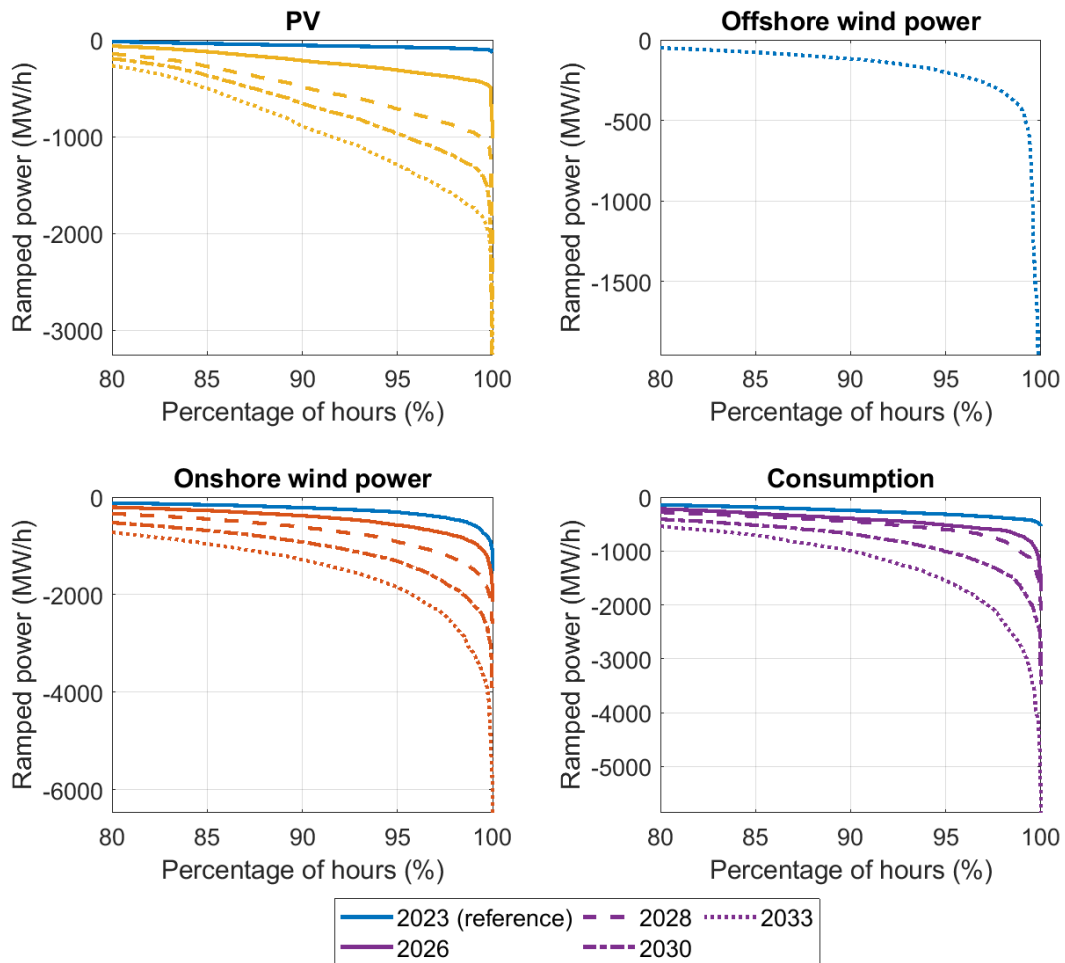


Figure 18: The last 20 % of the hourly ramping duration curves. Market simulation data used in this figure was created by applying mid-wind climate year. The reference duration curve is calculated from the historical measurement data of the year 2023. To distinguish the lines from each other, top 0.5 % downward ramping values from the year 2033 are excluded from the figures.

From the figures presented above, we can observe that the magnitudes of the PV ramps increase more linearly compared to wind power and consumption, when approaching 0 or 100 percent in the x-axes of the graphs. One possible explanation for this behavior is the partly deterministic nature of PV production driven by the cyclic movement between the Sun and Earth [27]. Consequently, the performed hourly analysis will not necessarily give best possible insight on the PV's ramping potential as the more challenging events tend to occur stochastically within the intra-hour level, due to the fast irradiation changes discussed earlier in sub-section 2.3.3.

The highest values in relation to the installed capacity are linked to offshore wind power. Nonetheless, this observation should not be given too much weight due to the small number of offshore parks modeled in the market simulations, leading to low geographical

aggregation [53]. The second highest relative ramps are associated to PV with maximums up to 40 % of the installed capacity (2030). The 90th and 10th percentiles of the PV ramps stay close to 7 % during all climate years and base cases. To give a reference point for the PV ramping, the maximum onshore wind power ramps stay below 29 % and the 90th and 10th percentiles are around 4-5 % with the same scope of analysis.

How much impact the presented consumption and production ramps will have on deterministic imbalances depends mainly on their respective ramping speeds. Traditionally, consumption has ramped more steadily compared to production and HVDC connections, creating momentary imbalances during MTU shifts [36]. However, this relationship may be reformed in the future, due to changes in both production and consumption side. For example, production's ramping behavior can be expected to become more distributed and stochastic around the MTU shifts, as the changes in weather-dependent production are often determined by the availability of wind or irradiation. This development may be opposite on the consumption side, if for example hydrogen production and electrical district heating actively follows the electricity price fluctuations and ramps quickly in the beginning of the MTU.

6. DISCUSSION

Since the balancing needs are highly system-specific, the figures presented in the previous chapter cannot be directly compared to the results of the recent integration studies [9][10][11], performed with different production and consumption structures. Also, comparing the estimated values to older Finnish studies, such as [103][104], is irrelevant due to their vastly outdated assumptions considering the system development. This comparison is further complicated by the differences in the used methodologies, reliability levels and modeled uncertainties. Because of the listed reasons, this chapter focuses on the meaning and validity of the obtained results.

How the balancing needs presented in the previous chapter will translate to the actual reserve procurement, can be understood through the upcoming FRR dimensioning methodology. In the most pessimistic assessment, the estimated balancing needs describe the reserve procurement related to the normal imbalances and the total amount of procured FRR would be equal to the sum of the estimated balancing needs and the reference incident of the period in question [63]. However, this assessment is likely too cautious due to the possible capacity sharing and imbalance netting between the load-frequency control areas.

Through sharing, part of the FRR dimensioned for the disturbances can be fulfilled by relying on the same reserve capacity as some other TSO [42][63]. This optimization is based on the low probability of both TSOs activating their full FRR capacity at the same time [42]. The extent in which the sharing of FRR for disturbances is possible depends on how much transmission capacity can be assumed to be available based on the historical ATC data and specified reliability level [63]. The imbalance netting, in a turn, reduces the FRR procurement related to the normal imbalances. As in the case of capacity sharing, also this reduction depends on the availability of cross-border transmission capacity. It is also good to acknowledge that sharing and imbalance netting are bounded by the general objectives of the FRR dimensioning, according to which the combined FRR capacity should cover the historical net imbalances of the Nordic synchronous area at least 99 % of the time and meet the frequency quality targets defined by the SOGL.

The methodology or reliability level applied by the TSOs while dimensioning the FRR for the normal imbalances may also differ from the one used in this work, making the above discussed connection between the estimated balancing needs and procurement at least partly non-trivial. Furthermore, it should be recognized that the applied calculation model

is based solely on forecast errors, while the renewed FRR dimensioning methodology considers as well the short-term variability and deterministic imbalances [63]. Also, when discussing the development of total FRR procurement, it is good to acknowledge the possible increase due to the special regulations. However, there are many uncertainties in this progress, since the mFRR is not the only tool used for the grid management, and new market and grid service fee-based solutions are under development [105].

The key uncertainty sources of the estimation process itself can be divided to five primary classes: optional parameters used in the calculation, representativeness and quality of the input data, processing of the data, statistical dependencies between the modeled uncertainties, and market model simulations. One practical example of the used free-choice parameters is the applied reliability level. For instance, performing the calculation with 95 % and 99 % reliability levels leads to differences of 310-370 MW between the average balancing needs, within the year 2026 and conservative sub-scenario. If a similar comparison is performed for the year 2033, the difference in the average balancing needs rises close to 1000-1250 MW. As a second example, the choice of the internal parameters of the different sub-scenarios has a major impact on the results. To give some reference, the average balancing needs would increase by 250-290 MW during the year 2026, if conservative sub-scenario would be more pessimistic about the BRPs' market behavior by using division of 70/30 for the day-ahead and 1-hour forecasts.

The first uncertainty arising from the input data is related to the current geographical positioning of the Danish PV and offshore wind power production. In practice, the statistical properties of the Danish forecast error data will likely differ from the ones related to the projected capacity of Finland, due to the differences in the geographical dispersion and installation sizes. Secondly, the capacity data used for the scaling of forecast errors is not updated in real time. This will in turn lead to distorted pu error distributions and results, when part of the production capacity included in the forecast error time series is missing from the capacity data of the same period.

Besides these factors, the invalid or missing samples in the forecast, measurement and capacity time series will naturally distort the analysis. For example, there is a systematic deficit in the PV forecast data presenting the early morning and evening hours, as the used 1-hour prediction horizon dataset was updated only during the daytime for most of the year 2021. This deficit will ultimately lead to reduced descriptiveness of the PDFs expressing similar conditions and thus bias the calculation's results. It is also important to note that using 1-hour ahead forecast data for the uncertainty modeling will not reflect the most active market behavior possible, as the continuous intra-day market allows trading also within the preceding hour. In addition to the previous highlights, using the

TSOs' forecast data to describe the aggregated forecast errors of the individual market actors (discussed with more detail in sub-section 4.2), is something that must be considered while analyzing the calculation's results.

The data processing related uncertainties can be roughly categorized to those arising from the editing and filtering of the input data, and those linked to the creation of conditional pu PDFs. Perhaps the most obvious uncertainty related to the first category is the use of synthetic forecasts, which is likely to bias the results in the direction of underestimating, for the reasons discussed earlier in sub-section 4.2.1. The distortion caused by the filtering, on the other hand, is related to the descriptiveness of the conditional PDFs. For example, in the case of wind power where the filtering is based on negative down-regulation prices, the data is systematically removed from the windy periods as the negative prices and high wind production levels tend to correlate.

From the PDF linked uncertainties, the first one is related to the feature scaling. To give an example, the features associated to pu production level vary over a wider range than the features related to pu power changes, making the production level more important feature during the clustering. As such, this can be seen as a property of the calculation model rather than a weakness, although it is good to acknowledge while analyzing the obtained results. The second PDF related uncertainty arises from the bandwidth selection within kernel density estimation, as it directly affects the smoothness and width of the created pu PDFs. For example, if standard deviation is used instead of median absolute estimator for the bandwidth selection, the average balancing needs decrease by 220-280 MW during the year 2026 and conservative sub-scenario. Finally, scaling with the annual peak demand, when using the production level as a feature, increases the sensitivity towards extreme events in the consumption data.

The fourth key uncertainty class originates from the assumption that the forecast error types, and their different prediction horizons are statistically independent. From these assumptions, especially the one concerning the independency between day-ahead and 1-hour forecasts, is challenging and must be acknowledged while analyzing the results. In practice this assumption begins to appear in the model's results as increased balancing needs, when the percentage of day-ahead forecasts is further reduced from the moderate and advanced sub-scenarios.

This counter-intuitive behavior can be explained through a hypothetical situation in which one would first calculate convolution for two error PDFs representing 50 % of the installed capacity, and then compare the obtained distribution to error PDF corresponding to full

capacity. In this comparison, the probability of larger errors is higher with the latter distribution, even though both density functions are upscaled from the same pu PDF. Since performing convolution with extremely narrow PDFs is effectively the same as not performing the operation at all, the presented hypothetical scenario will explain the observed increase, although the number of PDFs is kept constant during the actual calculation.

The same phenomenon can be observed also when repeating the calculation for a case in which the production and consumption uncertainties are modeled by using only forecast error data with 1-hour prediction horizon. The detailed results of this calculation can be found from Appendix B and C, but in short, they are of the same magnitude as those computed for the conservative sub-scenario. Similar calculation was also performed by assuming improved forecast accuracy and its results can be found from the same appendix. Besides to highlighting properties of the used methodology, these estimations will provide additional information about the development of the balancing needs that can be analyzed without having to consider the statistical dependency between the different forecast horizons.

At last, few market model related uncertainties are discussed briefly. Firstly, it is important to acknowledge that the used market simulation time series may not correspond to the hourly averages of market simulations created with 15-minute market resolution. Another point to consider is the large number of assumptions made during the initialization phase of the market model. To give an example, the thresholds for the curtailment of PV and wind production are directly reflected to the ramping values presented in subsection 5.3. Also, through a similar mechanism as in the case of the last PDF related uncertainty source, upscaling of the consumption error PDFs with the peak demand proposed by the market simulation results, increases the computations sensitiveness towards extreme events. Besides these factors, it is worth highlighting that as the market model assumes fixed production capacity throughout the simulated year, the upscaling of production's pu PDFs remains also unchanged. Consequently, the model is unable to describe the increase of the average balancing needs arising from the capacity development within the examined year.

7. CONCLUSION

The main objective of this work was to study the development of Finnish balancing needs during the years 2026-2033. This analysis was conducted through a case study, in which the development was assessed in three different sub-scenarios and climate years, representing variation in the BRPs' market behavior, forecast accuracy and wind conditions. Secondary objectives of this work were creating a process description for evaluating the development of balancing needs and estimating the growth potential of consumption and production ramping. The methodology applied in the case study was based on a probabilistic approach, in which the balancing needs were estimated from market simulation time series by using conditional forecast error distributions and predefined reliability level. The ramping of production and consumption, on the other hand, was studied by analyzing the market simulation data created originally for the case study.

When comparing the years 2026 and 2033, the predicted increase in the average balancing needs is about 320 % for the upward direction and close to 340 % for the downward direction. In this comparison, the reference year 2026 has around 800-1300 MW average balancing needs, depending on the applied sub-scenario, climate year and direction in question. From the modeled uncertainty sources, onshore wind power was found to be the main driver for the predicted growth and its impact was especially clear with the downward balancing needs. The largest absolute hourly ramping values were associated to the onshore wind power with maximums close to 28 % of the installed capacity. While performing similar comparison in relation to the installed capacity or peak demand, the offshore wind power and PV production rose to the top of the chart.

How the estimated balancing needs will reflect to the actual aFRR and mFRR procurement, depends on many factors such as possibility for reserve sharing, imbalance netting and accuracy of the forecast based mFRR activations. Nevertheless, it is important to acknowledge that due to the substantial predicted growth, relying solely on the reserve procurement made by the TSOs is hardly an economically viable option. For this reason, the role of self-balancing and intra-day trading of the BRPs will increase significantly in the coming years.

The capability for self-balancing could be enhanced by integrating energy storage systems as a standard component in all new wind and PV projects. Besides to technical solutions, operational decisions such as not selling all predicted wind production to cre-

ate a buffer for the possible forecast errors, is something that should be considered especially when the turbines are forecasted to operate below their nominal power. To incentivize this essential development, imbalance pricing could have an additional component which would increase the settlement price during challenging system conditions [9]. Also, since the geographical dispersion of the wind and PV assets increases the aggregation of forecast errors, it could be beneficial to guide the investment decisions through an additional component in the connection fees, analogous to one already proposed to optimize the use of existing grid [105].

In terms of achieving the set main and secondary objectives, this work can be considered highly successful. Also, the novelty value arising from the possibility to consider the effect of market behavior must be emphasized. However, due to the strict scope of the performed analysis and limitations related to the input data, the need for future research remains substantial. For example, it would be valuable to repeat the calculation after both forecast and market simulation data are available on 15-minute resolution. The applied methodology could be also further developed to consider the effect of imbalance netting and other uncertainty sources like deterministic imbalances and contingency events. Within this development work, it would be similarly beneficial to scope the impact of newer imbalance creation mechanisms such as large-scale icing of wind turbines leading to major forecast errors [106]. Finally, the correlations between the behavior of individual uncertainty sources and balancing needs could be studied in more detail.

SOURCES

- [1] N. Modig, R. Eriksson, P. Ruokolainen, J. N. Ødegård, S. Weizenegger, and T. D. Fechtenburg, "Overview of Frequency Control in the Nordic Power System," ENTSO-E, 2022. Accessed: Aug. 15, 2024. [Online]. Available: <https://www.epressi.com/media/userfiles/107305/1648196866/overview-of-frequency-control-in-the-nordic-power-system-1.pdf>
- [2] K. De Vos, N. Stevens, O. Devolder, A. Papavasiliou, B. Hebb, and J. Matthys-Donnadieu, "Dynamic dimensioning approach for operating reserves: Proof of concept in Belgium," *Energy Policy*, vol. 124, 2019, pp. 272–285, doi: 10.1016/j.enpol.2018.09.031.
- [3] European Union, *Commission Regulation (EU) 2017/1485 of 2 August 2017 establishing a guideline on electricity transmission system operation*. 2017. Accessed: Mar. 05, 2024. [Online]. Available: <http://data.europa.eu/eli/reg/2017/1485/2021-03-15/eng>
- [4] Affärsverket svenska kraftnät, Energinet, Fingrid Oyj, Kraftnät Åland AB, and Statnett SF, "System Operation Agreement between the Nordic Transmission System Operators (Nordic SOA)." 2019. Accessed: Mar. 05, 2024. [Online]. Available: https://eepublicdownloads.entsoe.eu/clean-documents/SOC%20documents/Nordic/Nordic%20SOA_Main%20Agreement.pdf
- [5] Nordic Operations Development Group, "Nordic Balancing Philosophy." ENTSO-E, 2021. Accessed: Feb. 22, 2024. [Online]. Available: <https://www.fingrid.fi/globalassets/dokumentit/fi/sahkomarkkinat/kehityshankkeet/balancing-philosophy-updated-211110.pdf>
- [6] Turvallisuuskomitea and Puolustusministeriö, "Sähköriippuvuus modernissa yhteiskunnassa," 2015. Accessed: Aug. 19, 2024. [Online]. Available: https://www.fingrid.fi/globalassets/dokumentit/fi/julkaisut/sahkoriippuvuus_modernissa_yhteiskunnassa_verkkojulkaisu.pdf
- [7] Energinet, Fingrid, Statnett, and Svenska kraftnät, "Nordic Grid Development Perspective 2023," 2023. Accessed: Mar. 14, 2024. [Online]. Available: https://www.fingrid.fi/contentassets/6457e50d0dee45a38d69f709d9cd4c87/svk_ngpd2023_a4_korr4.pdf
- [8] Ministry of the Environment, "Finland's national climate change policy." Accessed: Mar. 15, 2024. [Online]. Available: <https://ym.fi/en/finland-s-national-climate-change-policy>
- [9] Elia, "ADEQUACY AND FLEXIBILITY STUDY FOR BELGIUM 2024 - 2034." 2023. Accessed: Apr. 02, 2024. [Online]. Available: https://issuu.com/eliagroup/docs/adequacy_flexibility_study_for_belgium_2024-2034?fr=sOTBhNDYxOTUwMTY
- [10] Energinet, "OUTLOOK FOR ANCILLARY SERVICES 2023-2040," 2023. Accessed: Jul. 18, 2024. [Online]. Available: <https://en.energinet.dk/media/gieparrh/outlook-for-ancillary-services-2023-2040.pdf>
- [11] EU-SysFlex, "Technical Shortfalls for Pan European Power System with High Levels of Renewable Generation - D2.4." 2020. Accessed: Aug. 22, 2024. [Online]. Available: https://eu-sysflex.com/wp-content/uploads/2021/06/EU-SysFlex_D2.4_Scarcity_identification_for_pan_European_System_V1.0_For-Submission.pdf
- [12] L. Haarla and J. Elovaara, *Sähköverkot 1*, 2nd ed. Gaudeamus/Otatieto, 2011.
- [13] E. Ørum *et al.*, "Future System Inertia 2," ENTSO-E, 2017. Accessed: Aug. 15, 2024. [Online]. Available: <https://www.statnett.no/globalassets/for-aktorer-i-kraftsystemet/utvikling-av-kraftsystemet/nordisk-frekvensstabilitet/future-system-inertia-phase-2.pdf>
- [14] eSett Oy, "Nordic Imbalance Settlement Handbook." 2024. Accessed: Jan. 05, 2024. [Online]. Available: <https://www.esett.com/app/uploads/2023/12/NBS-Handbook-v4.6.pdf>
- [15] Työ- ja elinkeinoministeriö, *Sähkömarkkinalaki*. 2013. Accessed: Feb. 21, 2024. [Online]. Available: <https://finlex.fi/fi/laki/ajantasa/2013/20130588#O3L9P67>
- [16] Työ- ja elinkeinoministeriö, *Valtioneuvoston asetus sähkötoimitusten selvityksestä ja mittauksesta*. 2021. Accessed: Feb. 21, 2024. [Online]. Available: <https://finlex.fi/fi/laki/ajantasa/2021/20210767>
- [17] Fingrid Oyj, "Imbalance settlement." Accessed: Feb. 22, 2024. [Online]. Available: <https://www.fingrid.fi/en/electricity-market/balance-service/imbalance-settlement/>
- [18] Fingrid Oyj, "Liite 1: TASEVASTUUTA JA TASESELVITYSTÄ KOSKEVA KÄSIKIRJA - OSA 1: FINGRID OYJ:N YLEISET TASEHALLINNAN EHDOT." 2023. Accessed: Feb. 23,

2024. [Online]. Available: <https://www.fingrid.fi/globalassets/dokumentit/fi/sahkomarkkinat/tasesahko/voimaan-22.5.2023-01.00-liite-1-osa-1-fingrid-oyjn-yleiset-tasehallinnan-ehdot.pdf>
- [19] E. Lahtinen and H. Raatikainen, "Tasepoikkeaman hinnoittelu kesällä 2024," 2024. Accessed: Aug. 22, 2024. [Online]. Available: <https://www.fingrid.fi/globalassets/dokumentit/fi/sahkomarkkinat/tasesahko/webinaari-7.3.24-tasepoikkeaman-hinnoittelu-kesalla-2024.pdf>
- [20] J. Partanen, S. Annala, J. Lassila, and S. Honkapuro, *Sähkömarkkinat - opetusmoniste*. LUT University, 2020.
- [21] ACER, "Designation of NEMOs." Accessed: Aug. 27, 2024. [Online]. Available: <https://www.acer.europa.eu/electricity/market-rules/capacity-allocation-and-congestion-management/implementation/designation-of-nemos>
- [22] Fingrid Oyj, "Markkinapaikat." Accessed: Aug. 26, 2024. [Online]. Available: <https://www.fingrid.fi/sahkomarkkinat/markkinoiden-yhtenaisyys/johdanto-sahkomarkkinoihin/>
- [23] SIDC/MCSC, "Information Package About Intraday Auction - IDA." 2024. Accessed: Aug. 26, 2024. [Online]. Available: https://eepublicdownloads.blob.core.windows.net/public-cdn-container/clean-documents/Network%20codes%20documents/Implementation/cacm/xbid/IDAs-information_package-final.pdf
- [24] Fingrid Oyj, "Flow-based sidosryhmättilaisuus," Helsinki, 2023. Accessed: Mar. 19, 2024. [Online]. Available: <https://www.fingrid.fi/globalassets/dokumentit/fi/sahkomarkkinat/kehityshankkeet/flow-based-sidosryhmatilaisuus-21.11.2023.pdf>
- [25] J. Miettinen and H. Holttinen, "Impacts of wind power forecast errors on the real-time balancing need: a Nordic case study," *IET Renew. Power Gener.*, vol. 13, no. 2, 2019, pp. 227–233, doi: 10.1049/iet-rpg.2018.5234.
- [26] L. Hirth and I. Ziegenhagen, "Balancing power and variable renewables: Three links," *Renew. Sustain. Energy Rev.*, vol. 50, 2015, pp. 1035–1051, doi: 10.1016/j.rser.2015.04.180.
- [27] T. AISkaif, S. Dev, L. Visser, M. Hossari, and W. Van Sark, "A systematic analysis of meteorological variables for PV output power estimation," *Renew. Energy*, vol. 153, 2020, pp. 12–22, doi: 10.1016/j.renene.2020.01.150.
- [28] J. Miettinen and H. Holttinen, "Characteristics of day-ahead wind power forecast errors in Nordic countries and benefits of aggregation," *Wind Energy*, vol. 20, no. 6, 2017, pp. 959–972, doi: 10.1002/we.2073.
- [29] O. Anaya-Lara, N. Jenkins, J. B. Ekanayake, P. Cartwright, and M. Hughes, *Wind Energy Generation: Modelling and Control*. United Kingdom: John Wiley & Sons, Incorporated, 2009. Accessed: Feb. 28, 2024. [Online]. Available: <http://ebookcentral.proquest.com/lib/tampere/detail.action?docID=454292>
- [30] H. Holttinen et al., "Design and operation of energy systems with large amounts of variable generation," VTT, Espoo, 2021. Accessed: Feb. 01, 2024. [Online]. Available: <https://doi.org/10.32040/2242-122X.2021.T396>
- [31] H. Holttinen, J. Miettinen, and S. Sillanpää, "Wind power forecasting accuracy and uncertainty in Finland," VTT, Espoo, 2013. Accessed: Aug. 22, 2024. [Online]. Available: <https://publications.vtt.fi/pdf/technology/2013/T95.pdf>
- [32] D. Yang et al., "A review of solar forecasting, its dependence on atmospheric sciences and implications for grid integration: Towards carbon neutrality," *Renew. Sustain. Energy Rev.*, vol. 161, 2022, p. 112348, doi: 10.1016/j.rser.2022.112348.
- [33] K. Lappalainen and S. Valkealahti, "Sizing of energy storage systems for ramp rate control of photovoltaic strings," *Renew. Energy*, vol. 196, 2022, pp. 1366–1375, doi: 10.1016/j.renene.2022.07.069.
- [34] E. Nuno, M. Koivisto, N. A. Cutululis, and P. Sorensen, "On the Simulation of Aggregated Solar PV Forecast Errors," *IEEE Trans. Sustain. Energy*, vol. 9, no. 4, 2018, pp. 1889–1898, doi: 10.1109/TSTE.2018.2818727.
- [35] M. B. W. Hansen, B. M. Lumby, H. S. Næss-Schmidt, R. Beune, and B. Özalay, "Finer time resolution in Nordic power markets: A Cost Benefit Analysis," 2017. Accessed: Feb. 27, 2024. [Online]. Available: <https://www.fingrid.fi/globalassets/dokumentit/fi/sahkomarkkinat/varttitase/finer-time-resolution-cba-report-final-id-152439.pdf>
- [36] Energinet, Fingrid Oyj, Statnett, and Svenska kraftnät, "Explanatory document for the amended Nordic LFC block methodology for ramping restrictions for active power output in accordance with Article 137(3) and (4) of the Commission Regulation (EU) 2017/1485 of 2 August 2017 establishing a guideline on electricity transmission system operation." ENTSO-

- E, 2023. Accessed: Aug. 28, 2024. [Online]. Available: https://consultations.entsoe.eu/system-operations/nordic-tsos-methodology-for-ramping-restrictions-f/supporting_documents/230130%20Explanatory%20Document%20for%20Ramping%20restrictions%20for%20active%20power%20output%20amended%20for%20public%20consultation.pdf
- [37] V. Valli, “The impact of the market time unit shift production ramping on the power system balance,” Aalto University, 2022. Accessed: Aug. 28, 2024. [Online]. Available: <https://urn.fi/URN:NBN:fi:aalto-202206194098>
- [38] M. Talvi, T. Roinila, and K. Lappalainen, “Effects of Ramp Rate Limit on Sizing of Energy Storage Systems for PV, Wind and PV–Wind Power Plants,” *Energies*, vol. 16, no. 11, 2023, p. 4313, doi: 10.3390/en16114313.
- [39] J. Marcos, L. Marroyo, E. Lorenzo, and M. García, “Smoothing of PV power fluctuations by geographical dispersion,” in *Photovoltaics: Research and Applications*, 2012, pp. 226–237. doi: 10.1002/pip.1127.
- [40] Fingrid Oyj, “Olkiluoto 3 kantaverkossa.” Accessed: Aug. 28, 2024. [Online]. Available: <https://www.fingrid.fi/kantaverkko/sahkonsiirto/olkiluoto-3-kantaverkkoon/>
- [41] Statnett, “NordLink.” Accessed: Mar. 05, 2024. [Online]. Available: <https://www.statnett.no/en/our-projects/interconnectors/nordlink/>
- [42] Fingrid Oyj, Energinet, Svenska kraftnät, Statnett, and Kraftnät Åland AB, “Nordic System Operation Agreement (SOA) – Annex Load-Frequency Control & Reserves (LFCR).” 2023. Accessed: Jan. 05, 2024. [Online]. Available: https://eepublicdownloads.entsoe.eu/clean-documents/SOC%20documents/LFC/LFCR_annex_v5.pdf
- [43] Fingrid Oyj, Energinet, Svenska kraftnät, and Statnett, “Explanatory document for the Nordic synchronous area proposal for frequency quality defining parameters and the frequency quality target parameter in accordance with Article 127 of the Commission Regulation (EU) 2017/1485 of 2 August 2017 establishing a guideline on electricity transmission system operation.” ENTSO-E, 2018. Accessed: Aug. 28, 2024. [Online]. Available: https://consultations.entsoe.eu/markets/nordic-tsos-proposals-for-frequency-quality-and-fc/supporting_documents/Explanatory%20document%20for%20frequency%20quality%20proposal.pdf
- [44] Fingrid Oyj, Energinet, Svenska kraftnät, and Statnett, “Amended Nordic synchronous area methodology for the dimensioning rules for FCR in accordance with Article 153 of the Commission Regulation (EU) 2017/1485 of 2 August 2017 establishing a guideline on electricity transmission system operation.” ENTSO-E, 2022. Accessed: Aug. 28, 2024. [Online]. Available: https://consultations.entsoe.eu/system-operations/nordic-tsos-proposal-on-fcr-dimensioning/supporting_documents/153%20%20Nordic%20FCR%20dimensioning%20proposal.pdf
- [45] Fingrid Oyj, Energinet, Svenska kraftnät, and Statnett, “Nordic synchronous area proposal for the frequency quality defining parameters and the frequency quality target parameter in accordance with Article 127 of the Commission Regulation (EU) 2017/1485 of 2 August 2017 establishing a guideline on electricity transmission system operation.” ENTSO-E, 2018. Accessed: Aug. 28, 2024. [Online]. Available: https://consultations.entsoe.eu/markets/nordic-tsos-proposals-for-frequency-quality-and-fc/supporting_documents/Nordic%20frequency%20quality%20proposal.pdf
- [46] V. Eurasto, “Tuning of the load-frequency controller for the Finnish power system,” Aalto University, 2023. Accessed: Aug. 28, 2024. [Online]. Available: <https://urn.fi/URN:NBN:fi:aalto-202310156416>
- [47] Fingrid Oyj, Energinet, Svenska kraftnät, and Statnett, “Technical Requirements for Frequency Containment Reserve Provision in the Nordic Synchronous Area.” ENTSO-E, 2023. Accessed: Mar. 08, 2024. [Online]. Available: <https://www.fingrid.fi/globalassets/dokumentit/fi/sahkomarkkinat/reservit/appendix-2-the-technical-requirements-and-the-prequalification-process-of-frequency-containment-reserves-fcr.pdf>
- [48] Fingrid Oyj, “Frequency containment reserves (FCR products).” Accessed: Mar. 08, 2024. [Online]. Available: https://www.fingrid.fi/en/electricity-market/reserves_and_balancing/frequency-containment-reserves/
- [49] Fingrid Oyj, Energinet, Svenska kraftnät, and Statnett, “Roadmap and projects.” Accessed: Aug. 28, 2024. [Online]. Available: <https://nordicbalancingmodel.net/roadmap-and-projects/>
- [50] Fingrid Oyj, “BSP - Implementation Guide - aFRR energy market.” 2023. Accessed: Mar. 05, 2024. [Online]. Available: <https://www.fingrid.fi/globalassets/dokumentit/fi/sahkomarkkinat/reservit/implementation-guide-afrr-energy-activation-market.pdf>

- [51] Fingrid Oyj, Energinet, Svenska kraftnät, and Statnett, "Nordic mFRR capacity market." Accessed: Mar. 21, 2024. [Online]. Available: <https://nordicbalancingmodel.net/roadmap-and-projects/nordic-mfrr-capacity-market/>
- [52] Fingrid Oyj, "Prospects for future electricity production and consumption-FINGRID'S FORECAST Q1/2024," 2024. Accessed: Aug. 28, 2024. [Online]. Available: <https://www.fingrid.fi/globalassets/dokumentit/fi/kantaverkko/kantaverkon-kehittaminen/prospects-for-future-electricity-production-and-consumption-q1-2024-fingrid.pdf>
- [53] V. Salvi, "Fingrid planner interview," 2024.
- [54] Teollisuuden Voima Oyj, "TVO - Olkiluoto 1- ja Olkiluoto 2 -laitosyksiköiden käyttöiän pidennystä ja tehonkorotusta koskeva YVA-ohjelma on valmistunut." Accessed: Mar. 18, 2024. [Online]. Available: <https://www.tvo.fi/ajankohtaista/tiedotteetporssitiedotteet/2024/olkiluoto1-jaolkiluoto2-laitosyksikoidenkayttoianpidennystajatehonkorotustakoskevayva-ohjelmaonvalmistunut.html>
- [55] Energinet, Fingrid Oyj, Statnett, and Svenska kraftnät, "Solutions for a green Nordic energy system – Strategies to meet the climate challenge," 2022. Accessed: Mar. 14, 2024. [Online]. Available: <https://www.epressi.com/media/userfiles/107305/1645102507/solutions-report-2022.pdf>
- [56] Fingrid Oyj, "Aurora Line." Accessed: Jun. 11, 2024. [Online]. Available: <https://www.fingrid.fi/en/grid/construction/aurora-line/>
- [57] Members of MARI project, "MARI Activation Optimization Function Public Description." ENTSO-E, 2023. Accessed: Mar. 22, 2024. [Online]. Available: https://eepublicdownloads.blob.core.windows.net/public-cdn-container/clean-documents/Network%20codes%20documents/NC%20EB/2023/MARI_AOF_PublicDocumentation_v1.2.pdf
- [58] Fingrid Oyj, Energinet, Svenska kraftnät, and Statnett, "Explanatory document to all TSOs' proposal for the implementation framework for a European platform for the exchange of balancing energy from frequency restoration reserves with automatic activation in accordance with Article 21 of Commission Regulation (EU) 2017/2195 establishing a guideline on electricity balancing." ENTSO-E, 2018. Accessed: Mar. 21, 2024. [Online]. Available: https://eepublicdownloads.entsoe.eu/clean-documents/nc-tasks/EBGL/EBGL_A21_181218_ALL%20TSOs%20proposal_aFRRIF_explanatory_document_for%20submission.pdf
- [59] Fingrid Oyj, Energinet, Svenska kraftnät, and Statnett, "Automated mFRR energy activation market." Accessed: Mar. 22, 2024. [Online]. Available: <https://nordicbalancingmodel.net/roadmap-and-projects/automated-nordic-mfrr-energy-activation-market/>
- [60] Svenska kraftnät, Energinet, Fingrid Oyj, and Statnett, "Market Handbook - Nordic FRR capacity markets." Nordic Balancing Model, 2023. Accessed: Mar. 21, 2024. [Online]. Available: <https://nordicbalancingmodel.net/wp-content/uploads/2023/06/Market-handbook-FRR-CM.pdf>
- [61] Statnett, Fingrid Oyj, Energinet, and Svenska kraftnät, "The Way forward - Solutions for a changing Nordic power system," 2018. Accessed: Mar. 21, 2024. [Online]. Available: https://www.statnett.no/globalassets/om-statnett/nyheter-og-pressemeldinger/the-way-forward---solutions-for-a-changing-nordic-power-system_lowres.pdf
- [62] Fingrid Oyj, "mFRR- energiamarkkina webinaari," 2024. Accessed: Aug. 28, 2024. [Online]. Available: <https://www.fingrid.fi/globalassets/dokumentit/fi/tiedotteet/sahkomarkkinat/2024/mfrr-energiamarckkinawebinaari-20240314.pdf>
- [63] Fingrid Oyj, Energinet, Svenska kraftnät, and Statnett, "Amended Nordic LFC block methodology for FRR dimensioning in accordance with Article 157(1) of the Commission Regulation (EU) 2017/1485 of 2 August 2017 establishing a guideline on electricity transmission system operation." ENTSO-E, 2022. Accessed: Oct. 1, 2024 [Online]. Available: https://consultations.entsoe.eu/system-operations/nordic-tsos-proposal-on-frr-dimensioning/supporting_documents/20210907%20FRR%20dimensioning%20rules%20amendment%20proposal%20final%20TSO%20approved.pdf
- [64] Fingrid Oyj, Energinet, Svenska kraftnät, and Statnett, "Explanatory document for the amended Nordic LFC block methodology for FRR dimensioning in accordance with Article 157(1) of the Commission Regulation (EU) 2017/1485 of 2 August 2017 establishing a guideline on electricity transmission system operation." ENTSO-E, 2022. Accessed: Mar. 13, 2024. [Online]. Available: <https://consultations.entsoe.eu/system-operations/nordic->

- tsos-proposal-on-frr-dimensioning/supporting_documents/20210824%206_190513%20Explanatory%20document%20for%20FRR%20dimensioning%20rules%20final%20%20TSO%20approved.pdf
- [65] M. Bucksteeg, L. Niesen, and C. Weber, "Impacts of Dynamic Probabilistic Reserve Sizing Techniques on Reserve Requirements and System Costs," *IEEE Trans. Sustain. Energy*, vol. 7, no. 4, 2016, pp. 1408–1420, doi: 10.1109/TSTE.2016.2555483.
- [66] E. J. S. Del Rosario and J. R. C. Orillaza, "Dynamic Sizing of Frequency Control Ancillary Service Requirements for a Philippine Grid," presented at the 2023 IEEE Power & Energy Society General Meeting (PESGM), Orlando, FL, USA: IEEE, 2023, pp. 1–5. doi: 10.1109/PESGM52003.2023.10252643.
- [67] H. Holttinen *et al.*, "Methodologies to Determine Operating Reserves Due to Increased Wind Power," *IEEE Trans. Sustain. Energy*, vol. 3, no. 4, 2012, pp. 713–723, doi: 10.1109/TSTE.2012.2208207.
- [68] N. Menemenlis, M. Huneault, and A. Robitaille, "Computation of Dynamic Operating Balancing Reserve for Wind Power Integration for the Time-Horizon 1–48 Hours," *IEEE Trans. Sustain. Energy*, vol. 3, no. 4, 2012, pp. 692–702, doi: 10.1109/TSTE.2011.2181878.
- [69] A. F. Nematollahi and B. Vahidi, "The Application of the Cholesky-Based Monte Carlo Method to Evaluate Lightning Channel Base Current," *IEEE Trans. Electromagn. Compat.*, vol. 65, no. 3, 2023, pp. 804–811, doi: 10.1109/TEMC.2023.3265260.
- [70] Fingrid Oyj, "Estimations made by Fingrid's specialists." 2024.
- [71] Fingrid Oyj, "Fingrid's internal database." 2024.
- [72] C. Maurer, S. Krahl, and H. Weber, "Dimensioning of secondary and tertiary control reserve by probabilistic methods," *Eur. Trans. Electr. Power*, vol. 19, no. 4, 2009, pp. 544–552, doi: 10.1002/etep.326.
- [73] Energinet, "Forecast Wind and Solar Power, 5 min." Accessed: Apr. 24, 2024. [Online]. Available: https://www.energidataservice.dk/tso-electricity/Forecasts_5Min
- [74] D. Jost, M. Speckmann, F. Sandau, and R. Schwinn, "A new method for day-ahead sizing of control reserve in Germany under a 100% renewable energy sources scenario," *Electr. Power Syst. Res.*, vol. 119, 2015, pp. 485–491, doi: 10.1016/j.epsr.2014.10.026.
- [75] Fingrid Oyj, Energinet, Svenska kraftnät, and Statnett, "Explanatory document for the amended Nordic synchronous area proposal for ramping restrictions for active power output in accordance with Article 137(3) and (4) of the Commission Regulation (EU) 2017/1485 of 2 August 2017 establishing a guideline on electricity transmission system operation." EN-TSO-E, 2021. Accessed: Aug. 28, 2024. [Online]. Available: https://consultations.entsoe.eu/system-operations/nordic-tsos-proposal-on-ramping-restrictions/supporting_documents/210119%20Explanatory%20document%20for%20ramping%20restrictions%20amended%20for%20vs3.0%20for%20public%20consultation.pdf
- [76] Energinet, "Data Catalog - Energi Data Service." Accessed: Apr. 24, 2024. [Online]. Available: <https://en.energinet.dk/energy-data/data-catalog/>
- [77] Energinet, "Power System Right Now." Accessed: Apr. 24, 2024. [Online]. Available: <https://www.energidataservice.dk/tso-electricity/powersystemrightnow>
- [78] The Danish Energy Agency, "Master Data Register of Electric Generators," 2024.
- [79] The Danish Energy Agency, "Analyseforudsætninger til Energinet." Accessed: May 07, 2024. [Online]. Available: <https://ens.dk/service/fremskrivninger-analyser-modeller/analyseforudsatninger-til-energinet>
- [80] Fingrid Oyj, "Open data on the electricity market and the power system." Accessed: Apr. 24, 2024. [Online]. Available: <https://data.fingrid.fi/en>
- [81] Motiva and energiavirasto, Aurinkosähkövoimalat. Accessed: May 08, 2024. [Online]. Available: <https://aurinkosahkovoimalat.fi/>
- [82] The Danish Energy Agency, "Power Production and Transmission in Denmark," 2019. Accessed: Jul. 29, 2024. [Online]. Available: https://ens.dk/sites/ens.dk/files/Analyser/el_infrastruktur_201907_eng.pdf
- [83] Nord Pool, "Day-Ahead Market Data." Accessed: Apr. 25, 2024. [Online]. Available: <https://www.nordpoolgroup.com/en/services/power-market-data-services/day-ahead-market-data/>
- [84] Copernicus Atmosphere Monitoring Service, "CAMS solar radiation time-series." 2024. Accessed: Jan. 07, 2024. [Online]. Available: <https://ads.atmosphere.copernicus.eu/cdsapp#!/dataset/cams-solar-radiation-timeseries?tab=overview>

- [85] Fingrid Oyj, Energinet, Svenska kraftnät, and Statnett, “ACE Open Loop and Imbalance forecast.” Accessed: Jun. 07, 2024. [Online]. Available: https://nordic-balancing.pages.fifty.eu/information/TSO-TSO/BusinessRequirementSpecification/aceol/index.html#_area_control_error_open_loop_ace_ol_and_imbalance_forecast
- [86] Fingrid Oyj, “Solar power generation forecast - updated every 15 minutes.” Accessed: Jul. 29, 2024. [Online]. Available: <https://data.fingrid.fi/en/datasets/248>
- [87] J. Buck, “Forecast models used by Energinet,” 2024.
- [88] Fingrid Oyj, “Terms and conditions for providers of manual Frequency Restoration Reserves (mFRR).” 2023. Accessed: Aug. 28, 2024. [Online]. Available: <https://www.fingrid.fi/globalassets/dokumentit/fi/sahkomarkkinat/saatosahko/liite-1-mfrr-ehdot-4-2022-hyvaksytyt-ehdot-en.pdf>
- [89] Suomen uusiutuvat, “Uusiutuvan energian tukeminen.” Accessed: Aug. 28, 2024. [Online]. Available: <https://tuulivoimayhdistys.fi/tietoa-tuulivoimasta-2/tietoa-tuulivoimasta/taloudellisuus/uusiutuvan-energian-tukeminen>
- [90] H. Kanerva, “Fingrid planner interview,” 2024.
- [91] Fingrid Oyj, “Sähkömarkkinoilla erikoinen tilanne perjantaina – hinta ei ohjaa tuotantoa ja kulutusta oikein.” Accessed: May 03, 2024. [Online]. Available: <https://www.fingrid.fi/ajankohtaista/tiedotteet/2023/sahkomarkkinoilla-erikoinen-tilanne-perjantaina--hinta-ei-ohjaa-tuotantoa-ja-kulutusta-oikein/>
- [92] S. Mäki-Turja, “Frequency quality analysis 2023,” Fingrid Oyj, 2024.
- [93] D. Arthur and S. Vassilvitskii, “k-means++: The Advantages of Careful Seeding,” in *Proceedings of the eighteenth annual ACM-SIAM symposium on Discrete algorithms*, 2007, pp. 1027–1035. Accessed: Sep. 20, 2024. [Online]. Available: <https://dl-acm-org.lib-proxy.tuni.fi/doi/abs/10.5555/1283383.1283494>
- [94] L. Kliemann and P. Sanders, Eds., *Algorithm Engineering - Selected Results and Surveys*. Springer International Publishing, 2016. doi: 10.1007/978-3-319-49487-6.
- [95] S. L. Mirtaheri and R. Shahbazian, *Machine Learning*. CRC Press, 2022. Accessed: May 02, 2024. [Online]. Available: <https://learning.oreilly.com/library/view/machine-learning/9781000737721/>
- [96] I. Faran, “CRPS — A Scoring Function for Bayesian Machine Learning Models.” Accessed: Jun. 10, 2024. [Online]. Available: <https://towardsdatascience.com/crps-a-scoring-function-for-bayesian-machine-learning-models-dd55a7a337a8>
- [97] T. Gneiting and A. E. Raftery, “Strictly Proper Scoring Rules, Prediction, and Estimation,” *J. Am. Stat. Assoc.*, vol. 102, no. 477, 2007, pp. 359–378, doi: 10.1198/016214506000001437.
- [98] The MathWorks, Inc., “Kernel Distribution.” Accessed: May 07, 2024. [Online]. Available: <https://www.mathworks.com/help/stats/kernel-distribution.html#btwcai2-3>
- [99] B. W. Silverman, *Density Estimation for Statistics and Data Analysis*. London: Chapman and Hall Ltd, 1986.
- [100] M. Wahbah, B. Mohandes, T. H. M. EL-Fouly, and M. S. El Moursi, “Unbiased cross-validation kernel density estimation for wind and PV probabilistic modelling,” *Energy Convers. Manag.*, vol. 266, 2022, p. 115811, doi: 10.1016/j.enconman.2022.115811.
- [101] A. Azzalini and A.W. Bowman, *Applied Smoothing Techniques for Data Analysis: The Kernel Approach with S-Plus Illustrations*. Oxford: Oxford University Press, 1997.
- [102] P. Cunningham and S. J. Delany, “k-Nearest Neighbour Classifiers - A Tutorial,” *ACM Comput. Surv.*, vol. 54, no. 6, 2021, doi: 10.1145/3459665.
- [103] Pöyry Management Consulting, “Demand and Supply of Flexibility,” 2018. Accessed: Aug. 28, 2024. [Online]. Available: https://www.fingrid.fi/globalassets/dokumentit/fi/sahkomarkkinat/kehityshankkeet/dalyve-fingrid_flexibility-study_final-report_v300-id-151641.pdf
- [104] L. Laitinen, “Tunninsisäinen tehotasapaino Suomessa 2020 ja 2030,” LUT University, 2013. Accessed: Sep. 20, 2024. [Online]. Available: <https://urn.fi/URN:NBN:fi-fe201305283746>
- [105] Fingrid Oyj, “Kantaverkkomaksujen muutosehdotukset,” 2024. Accessed: Aug. 07, 2024. [Online]. Available: <https://www.fingrid.fi/globalassets/dokumentit/fi/tiedotteet/ajankoh-taista/kantaverkkomaksujen-uudistusehdotukset-sidosryhmatilaisuus-14.6.2024.pdf>
- [106] J. Ämmälä, “Fingrid specialist interview,” 2024.

APPENDIX A: HOURLY BALANCING NEEDS

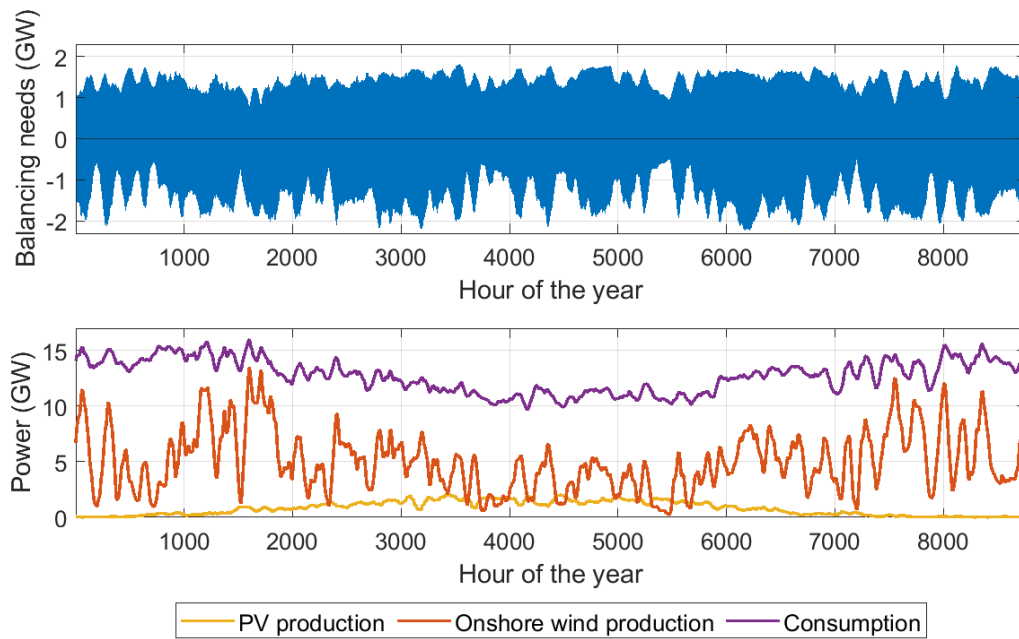


Figure 19: The upper graph presents hourly balancing needs for the year 2028 while applying moderate sub-scenario and mid-wind climate year. Positive values indicate upward balancing needs and negative values correspond to downward balancing needs. The lower graph illustrates production and consumption values of the same scenario. Since plotting the unfiltered time series would make the figure hard to interpret, 72 hour moving averages of the related time series are used instead.

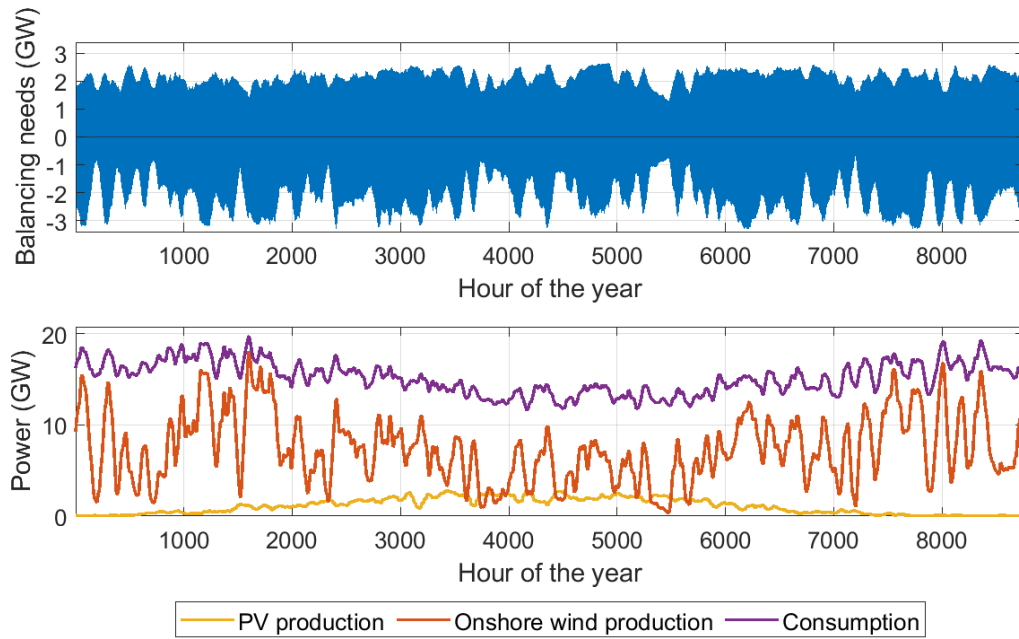


Figure 20: The upper graph presents hourly balancing needs for the year 2030 while applying moderate sub-scenario and mid-wind climate year. Positive values indicate upward balancing needs and negative values correspond to downward balancing needs. The lower graph illustrates production and consumption values of the same scenario. Since plotting the unfiltered time series would make the figure hard to interpret, 72 hour moving averages of the related time series are used instead.

APPENDIX B: BALANCING NEED CALCULATION WITHOUT DAY-AHEAD FORECASTS

Table 5: Minimum, average, and maximum upward balancing needs within different climate years. The left sub-scenario describes balancing needs while the forecast errors are modeled by using only 1-hour prediction horizon forecast data. The second sub-scenario differs from the first one by considering also the forecast accuracy development. The numerical values under the sub-scenario column are expressed in MW.

Base case	Climate year	Sub-scenarios					
		Only 1-h forecasts			Only 1-h forecasts + 25 % improvement in wind and PV forecast accuracy		
		Min	Avg	Max	Min	Avg	Max
2026	Low wind	312	1219	2556	206	952	1935
	Mid wind	547	1257	2559	445	981	1943
	High wind	501	1260	2711	424	983	2047
2028	Low wind	625	1874	4744	434	1440	3576
	Mid wind	729	1905	4841	504	1464	3643
	High wind	822	1920	4808	647	1476	3611
2030	Low wind	857	2763	6843	593	2104	5157
	Mid wind	846	2882	6482	586	2193	4874
	High wind	855	2943	7070	590	2241	5311
2033	Low wind	1039	3798	9471	694	2853	7126
	Mid wind	1039	4048	9110	692	3057	6855
	High wind	1132	4195	9751	764	3174	7320

Table 6: Minimum, average, and maximum downward balancing needs within different climate years. The left sub-scenario describes balancing needs while the forecast errors are modeled by using only 1-hour prediction horizon forecast data. The second sub-scenario differs from the first one by considering also the forecast accuracy development. The numerical values under the sub-scenario column are expressed in MW.

Base case	Climate year	Sub-scenarios					
		Only 1-h ahead forecasts			Only 1-h ahead forecasts + 25 % improvement in wind and PV forecast accuracy		
		Min	Avg	Max	Min	Avg	Max
2026	Low wind	202	1126	3585	204	881	2711
	Mid wind	208	1228	3671	206	953	2765
	High wind	248	1327	3581	243	1027	2702
2028	Low wind	288	1802	5485	255	1384	4130
	Mid wind	253	1898	5423	242	1452	4085
	High wind	300	2055	5441	286	1569	4096
2030	Low wind	390	2623	8100	358	2004	6080
	Mid wind	400	2918	8129	368	2223	6114
	High wind	397	3152	8125	369	2393	6112
2033	Low wind	529	3886	11621	489	2995	8692
	Mid wind	580	4245	11554	533	3242	8686
	High wind	564	4562	11650	512	3467	8745

APPENDIX C: BALANCING NEED CALCULATION WITHOUT DAY-AHEAD FORECASTS, DURATION CURVES OF THE RESULTS

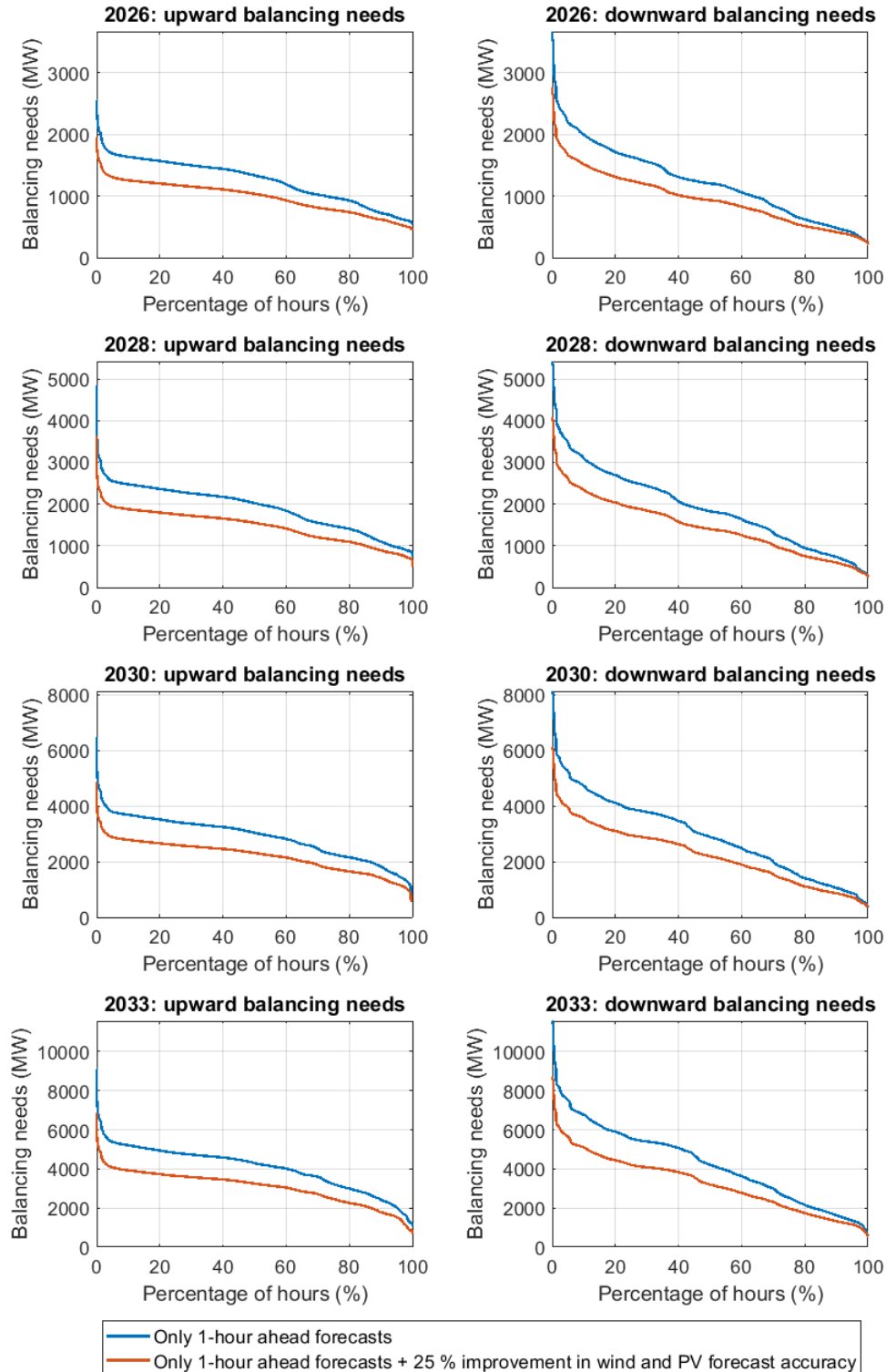


Figure 21: Duration curves of the estimated balancing needs within different years, while only 1-hour ahead forecasts are used for the modeling process. The market simulation data used for the calculation of the presented balancing needs was created by applying mid-wind climate year.